Journal of Hydrology: Regional Studies 37 (2021) 100903

Contents lists available at ScienceDirect

Journal of Hydrology: Regional Studies

journal homepage: www.elsevier.com/locate/ejrh

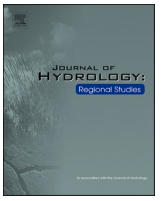

Evaluation of pedotransfer functions for predicting soil hydraulic properties: A voyage from regional to field scales across Europe

P. Nasta [a,*], B. Szabó [b], N. Romano [a]

[a] Department of Agricultural Sciences, AFBE Division, University of Naples Federico II, Portici, Naples, Italy
[b] Institute for Soil Sciences, Centre for Agricultural Research, Herman Ottóút 15, 1022, Budapest, Hungary

ARTICLE INFO

Keywords:
Water retention function
Saturated hydraulic conductivity
Semi-variogram
Kriging
Functional evaluation
Hydrus-1D

ABSTRACT

Study region: Europe. A total of 660, 522, and 4940 soil samples belonging to GRIZZLY, HYPRES, and EU-HYDI databases, respectively, were used for parametric evaluation.
Study focus: The soil water retention and hydraulic conductivity functions are crucial input information for land surface models. Determining these functions by using direct methods is hampered by excessive time and unaffordable costs required for field activities and laboratory analyses. Pedotransfer functions (PTFs) are widely-used indirect techniques enabling soil hydraulic properties to be predicted by using easily-retrievable soil information. In a parametric evaluation, the predictive capability of PTFs is examined by comparing measured and estimated soil water retention parameters and saturated hydraulic conductivity. Yet information about the performance of PTFs for specific modeling applications is mandatory to evaluate PTF effectiveness in greater depth. This approach is commonly defined as functional evaluation.
New hydrological insights for the region: The best performing four PTFs selected in the parametric evaluations are tested under two functional evaluations. The first encompasses a spatial interpolation with a geostatistical technique, whereas the second employs Hydrus-1D to simulate the water balance components along an experimental transect. Our results reinforce and integrate the insights of previous studies about the use of a PTF, and highlight the ability, or inability, of this technique to adequately reproduce the observed spatial variability of soil hydraulic properties and simulated water fluxes.

1. Introduction

Modeling large-scale soil water balance for applications in, for instance, irrigation, groundwater recharge, or sustainable water resources management, requires massive input data of the water retention function (WRF) and saturated hydraulic conductivity (K_s). Direct measurements of WRF are generally determined by conventional laboratory techniques using the hanging water column or the suction tables (Dane and Hopmans, 2002). The constant- or falling-head method is commonly used for measuring K_s (Reynolds and Elrick, 2002). The simultaneous determination of WRF and hydraulic conductivity function (HCF) via inverse modeling (transient-flow experiments) is often carried out in the laboratory using composite equipment that is used to impose a multi-step outflow or an evaporation process in a soil sample. Leaving aside for the time being the issue of in-situ experiments, together with the endless debate between field and laboratory tests, so far the hydrological community has considered the above-mentioned laboratory techniques as

* Corresponding author.
E-mail address: paolo.nasta@unina.it (P. Nasta).

https://doi.org/10.1016/j.ejrh.2021.100903
Received 16 February 2021; Received in revised form 3 August 2021; Accepted 30 August 2021
Available online 3 September 2021

precise and reliable (Hopmans et al., 2002; Schelle et al., 2010). However, despite several attempts at simplification (Schindler and Müller, 2006; Peters and Durner, 2008; Figueras and Gribb, 2009; Nasta et al., 2011), these approaches are still expensive, tedious, and time-consuming. Hence their use remains quite unrealistic for large-scale applications.

PTFs are statistical tools that relate soil hydraulic properties ("estimands") to easily measurable soil physico-chemical parameters ("predictors") (Guber et al., 2006; Van Looy et al., 2017). The availability of recent global-scale digital maps of soil physical and chemical properties provides high-quality and detailed (high-spatial-resolution) information to support the implementation of PTFs for modeling applications, such as SoilGrids 250 m (Hengl et al., 2017), and its recently updated version, SoilGrids 2.0 (Batjes et al., 2020; de Sousa et al., 2021).

Four main groups/categories of PTFs exist (Tietje and Tapkenhinrichs, 1993). The first group of PTFs proposes look-up tables (called class PTFs) listing average parameters in each texture class. Nonetheless, the recent availability of basic soil physical and chemical properties at a very high spatial resolution can make this type of PTF obsolete. In fact, the use of average parameters in a soil texture class oversimplifies model parameterization by completely missing the spatial variability over a study area. The second group of PTFs (called point PTFs) estimates soil water contents at fixed matric head values, such as field capacity and wilting point (Petersen et al., 1968; Gupta and Larson, 1979; Rawls et al., 1982; Canarache, 1993; Bruand et al., 1994). The third group of PTFs (called semi-physical PTFs) comprises physically sound (but semi-empirical) models based on the assumption of shape similarity between the particle-size distribution and pore-size distribution (Arya and Paris, 1981; Haverkamp and Parlange, 1986; Nimmo et al., 2007; Mohammadi and Vanclooster, 2011; Mohammadi and Meskini-Vishkaee, 2013). The fourth group of PTFs (called parameter PTFs) is based on the data-driven estimation of parameters featuring in the most widespread WRF equations (van Genuchten, 1980; Brooks and Corey, 1964) with multiple regression equations or more complex machine-learning approaches, such as artificial neural networks, support vector machines, and random forest (Rudiyanto et al., 2021). In general, multiple linear regression is often used for developing a PTF in an analytical form that can then be easily implemented by other users. PTFs derived by machine learning techniques often outperform the predictions obtained by the multiple linear regression, but can be used by other researchers only if they are built in a user-friendly platform (Zhang and Schaap, 2017; Araya and Ghezzehei, 2019; Szabó et al., 2021).

The predictive capability of a PTF is commonly tested by a parametric evaluation that analyzes the errors between measured and PTF-predicted soil hydraulic properties. However, a parametric evaluation would not necessarily provide information about the performance of a PTF when its predictions should be employed for computer modeling simulations. Beyond parametric accuracy and precision, it is therefore recommended to use functional criteria to compare model outputs when soil behavior is parameterized by using either measured or predicted soil hydraulic properties. For this reason, Vereecken et al. (1992) defined functional evaluation as "*the statistical examination of the variability in the outcome of a simulation model for a specific application when the variability arises solely from uncertainty in the PTFs*". Large-scale model applications depend on PTF quality, hence on the impact of epistemic uncertainties associated with the spatial variations of predicted soil hydraulic properties or the water fluxes simulated by a hydrological model. As pointed out by Pringle et al. (2007), another issue requiring due attention is the selection of the most suitable spatial scale in which a certain PTF can provide optimal performances.

In the wake of the paper written by Pringle et al. (2007) and allowing for the recent progress in the development of PTFs, this study aims primarily to investigate the ability of a PTF to reproduce adequately the observed variations in soil hydraulic parameters over a range of spatial scales from relatively large areas to transects. The impact of epistemic errors introduced when using a PTF in land surface models is mostly unknown, but any effort should be made to reduce them (Beven, 2013). For this reason, due consideration should be given to assessing model uncertainty at least in practical field-scale modeling applications.

The objective of this study is twofold: *i*) using a parametric evaluation to critically revise a set of existing PTFs on three large European soil hydraulic data sets to select the best-performing ones, which are subsequently tested under a functional perspective; *ii*) running two functional evaluations to analyze the epistemic errors generated when PTF-predicted soil hydraulic properties are used instead of those directly measured.

2. Materials and methods

2.1. Inventory of existing pedotransfer functions

2.1.1. Estimation of soil water retention function (WRF)

The WRF, $\theta(\psi)$, relates the volumetric soil water content, θ($cm^3\ cm^{-3}$), to soil matric head, ψ (cm). Among several options, the most widespread equation describing the WRF is the van Genuchten model (hereafter referred to as vG; van Genuchten, 1980; Li et al., 2014):

$$\theta(\psi) = \theta_r + \frac{\theta_s - \theta_r}{[1 + (\alpha\psi^n)]^m} \quad \text{with} \quad m = 1 - 1/n \tag{1}$$

where θ_r ($cm^3\ cm^{-3}$) and θ_s ($cm^3\ cm^{-3}$) are the residual and saturated soil water contents, respectively, α (cm^{-1}) is a scale parameter, and m (-) and n (-) are shape parameters. θ_s is measured according to the protocol suggested by Topp and Ferré (2002) and is slightly lower than soil porosity, *por*, as calculated through the following equation (Kotlar et al., 2019):

$$por = 1 - \frac{\rho_b}{\rho_d} \tag{2}$$

Table 1
List of eleven PTFs tested in three European databases.

PTF	Reference	Location of training data	Type of WRC model *	Type of the PTF**	Input variables of selected PTFs						
					sand %	silt %	clay %	ρ_b g cm^{-3}	OM %	soil depth cm	topsoil
SAX86	Saxton et al. (1986)	USA	–	pseudo-continuous, LR	+		+				
C&S92	Campbell and Shiozawa (1992)	Washington (USA)	BC	parametric, LR		+	+	+			
R&B85	Rawls and Brakensiek (1985)	USA	BC	parametric, LR	+		+	+			
O&C80	Oosterveld and Chang (1980)	Alberta, (Canada)	–	pseudo-continuous, LR	+		+	+		+	
WOS99	Wösten et al. (1999)	Europe	VG	parametric, LR		+	+	+	+		+
VER89	Vereecken et al. (1989)	Belgium	VG	parametric, LR	+		+	+	+		
euptfv2	Szabó et al. (2021)	Europe	VG	parametric, RF	+	+	+	+/-	+/-	+	
WEY09	Weynants et al. (2009)	Belgium	VG	parametric, LR	+		+	+	+		
ROSETTA	Schaap et al. (2001)	Europe and North America	VG	parametric, NN	+	+	+	+			
T&H98	Tomasella and Hodnett (1998)	Amazonia, Brazil	–	point (9 prescribed ψ-values), LR		+	+		+		
RAW82	Rawls et al. (1982)	USA	–	point (12 prescribed ψ-values), LR	+	+	+	+	+		

+/- denotes optional.
* Type of model for the description of the water retention curve: BC: Brooks and Corey (1964) model, VG: van Genuchten (1980) model.
** LR: linear regression, RF: random forest, NN: neural network, pseudo-continuous PTF: uses matric head as input variable by predicting the soil water content at any matric head value without applying any WRC models (Haghverdi et al., 2012).

where ρ_b is the oven-dry soil bulk density (g cm^{-3}), and ρ_d is the particle density (g cm^{-3}) assumed on average to be equal to 2.65 g cm^{-3}. The degree of saturation is defined as $S_e = (\theta\text{-}\theta_r)/(\theta_s\text{-}\theta_r)$ and varies from 0 ($\theta = \theta_r$) to 1 ($\theta = \theta_s$).

Knowledge of the WRF enables to determine two key soil hydraulic parameters of bucket-type hydrological models (Romano et al., 2011). The first parameter is the soil water content at the permanent wilting point, θ_{WP}, which is commonly computed as θ at the matric head $\psi = -15{,}300$ cm (i.e. a soil matric head of 15 bars), but the validity of this threshold for different plant species is still under debate (Torres et al., 2021). The second parameter is the soil water content at the condition of field capacity, θ_{FC} (field capacity value, for short), defined as the mean soil water content measured over the entire rooting zone of a soil profile when the water flux at its lower boundary becomes virtually nil during a drainage process (Romano and Santini, 2002). Alternatively, the field capacity value can be obtained in a virtual soil profile where the drainage process is properly described by a Richards-based hydrological model (Twarakavi et al., 2009; Nasta and Romano, 2016). For the sake of simplicity, θ_{FC} is often estimated at a fixed soil matric head (e.g. −500 cm, or −330 cm, or −100 cm), depending mainly on the dominant soil textural class in the soil profile (Romano et al., 2011). The θ_{FC} value can also be conveniently estimated through the following physically-based analytical equation proposed by Assouline and Or (2014):

$$\theta_{FC} = \theta_r + (\theta_s - \theta_r)\left\{1 + \left[\frac{n-1}{n}\right]^{(1-2n)}\right\}^{\left(\frac{1-n}{n}\right)} \quad (3)$$

that is based on the soil drainage dynamics and makes use of the parameters featuring in the vG equation of the WRF.

The hydraulic conductivity function (HCF) describes the ability of the soil to transfer water into the soil zone and relates the soil hydraulic conductivity, K (cm d^{-1}), to the volumetric soil water content, θ, or the soil matric head, ψ. The HCF is commonly described by the following vG-based parametric relation (van Genuchten, 1980):

$$K(S_e) = K_s S_e^{\tau}\left[1 - \left(1 - S_e^{1/m}\right)^m\right]^2 \quad (4)$$

where K_s (cm d^{-1}) is the saturated hydraulic conductivity, τ (-) represents the tortuosity parameter, commonly fixed at $\tau = 0.5$ (Mualem, 1976) or $\tau = -1$ (Schaap and Leij, 2000), but should be constrained to assure monotonicity of the HCF (Peters et al., 2011). The five unknown soil hydraulic parameters (α, n, θ_r, θ_s, and K_s) featuring in the vG WRF and the HCF should be directly measured (θ_s, and K_s) or fitted (α, n, and θ_r) to measurements.

In this study, we tested eleven PTFs belonging to both point and parametric models (see the list in Table 1) by ignoring those referred to as class or semi-physical models (Van Looy et al., 2017).

The WEY09 model was presented by Weynants et al. (2009) and subsequently corrected in Weihermüller et al. (2017). ROSETTA is

Table 2
List of ten PTFs tested in three European databases for estimating K_s.

PTF	Reference	Location of training data	Type of PTF*	Input variables of selected PTFs						
				sand %	silt %	clay %	ρ_b g cm^{-3}	OM %	soil depth cm	topsoil
WOS99	Wösten et al. (1999)	Europe	LR		+	+	+	+		+
euptfv2	Szabó et al. (2021)	Europe	RF	+	+	+	+/-	+/-	+	
ROSETTA	Schaap et al. (2001)	Europe and North America	NN	+	+	+	+			
A&G19	Araya and Ghezzehei (2019)	USA	BRT	+	+	+	+/-	+/-		
GUP20	Gupta et al. (2021)	global	LR	+		+	+			
COS84	Cosby et al. (1984)	USA	LR	+		+				
S&R06	Saxton and Rawls (2006)	USA	LR	+		+		+		
VER89 & GUA07	Vereecken et al. (1989), Guarracino (2007)	Belgium, USA	LR	+		+	+	+		
R&B85 & NAS13	Rawls and Brakensiek (1985), Nasta et al. (2013)	USA, Europe	LR	+		+	+			
WEY09 & GUA07	Weynants et al. (2009), Guarracino (2007)	Belgium, USA	LR	+		+	+	+		

+/- denotes optional.
*LR: linear regression, RF: random forest, NN: neural network, BRT: boosted regression tree.

based on a machine-learning approach (artificial neural network) but it is easy to use because it is implemented in Hydrus-1D (Šimůnek et al., 2018) and unknown parameters can be manually derived for each soil sample. WOS99 and euptfv2 are based on European data while ROSETTA is based on a data set of soil samples collected mainly in North America. WOS99, VER89, euptfv2, WEY09, and ROSETTA employ the parameters of van Genuchten's analytical relation. R&B85 predicts parameters of the Brooks and Corey (1964) model and considers soil porosity which was calculated by Eq. (2). We recall that C&S92, SAX86, and O&C80 adopt different analytical WRF equations. The last two point PTFs (T&H98 and RAW82) are based on tabulated regression coefficients at fixed matric head values (see Appendix A).

2.1.2. *Estimation of saturated hydraulic conductivity*

K_s is predicted by ten PTFs reported in Table 2. Zhang and Schaap (2019) provided a comprehensive review of methods to estimate K_s, and the COS84, and S&R06 relations were taken from their Appendix A. Seven methods – WOS99, euptfv2, ROSETTA, A&G19, GUP20, COS84, and S&R06 – are based on an empirical relationship between K_s and easily available soil properties.

In the case of three methods – VER89 & GUA07, R&B85 & NAS13, and WEY09 & GUA07 – K_s is computed from parameters of the WRF, which were previously predicted from basic soil properties. Guarracino (2007) (GUA07) proposed an equation to derive K_s from the knowledge of the vG water retention parameters as follows:

$$K_s = 4.65 \bullet 10^4 \theta_s \alpha^2 \tag{5}$$

when K_s is expressed in units of cm d^{-1}. Eq. (5) is applied to the VER89 and WEY09.

Another option is to use the physically-based relation proposed by Nasta et al. (2013) (NAS13) based on a simple capillary bundle model (Laliberte et al., 1968) that estimates K_s by using the WRF parameters of the Brooks and Corey (1964) equation:

$$K_s = 3.17 \bullet 10^5 \frac{\lambda}{\lambda + 2} \frac{\theta_s}{\psi_b^2} \tag{6}$$

Despite the criticism raised on the empirical meaning of the tortuosity parameter, Ghanbarian et al. (2017) proved that Eq. (6) performs satisfactorily based on its application on a large independent database from the USA. Eq. (6) is applied to R&B85 PTF which predicts the parameters (λ and ψ_b) of the Brooks and Corey model (see Eq. (A4) in the Appendix A).

2.2. *Soil databases*

In this study we evaluated PTF performance mainly for soils under a temperate climate by using the data stored in the Grenoble soil catalog GRIZZLY (Haverkamp et al., 1997), the Hydraulic PRoperties of European Soils (HYPRES) database (Wösten et al., 1999; Lilly et al., 2008) and the European HYdropedological Data Inventory (EU-HYDI) dataset (Weynants et al., 2013). Since all three databases were obtained from regional datasets there is, or might be, some overlap between them and the training data of the PTFs analyzed in this paper. Therefore, evaluation of the general performance –and no validation – could be performed on them to pre-select a smaller set of the PTFs for functional analysis. The GRIZZLY data set comprises a total of 660 soil samples (382 samples originating from Europe, 249 samples from the United States, and 31 samples outside Europe and the United States). Out of 4030 available soil samples in HYPRES, 541 were provided by the database organizers. We removed 19 soil samples and considered 522 soil samples belonging to HYPRES for our data analysis. In the case of the EU-HYDI we selected 4940 data for WRF out of 14,182 soil samples by omitting the

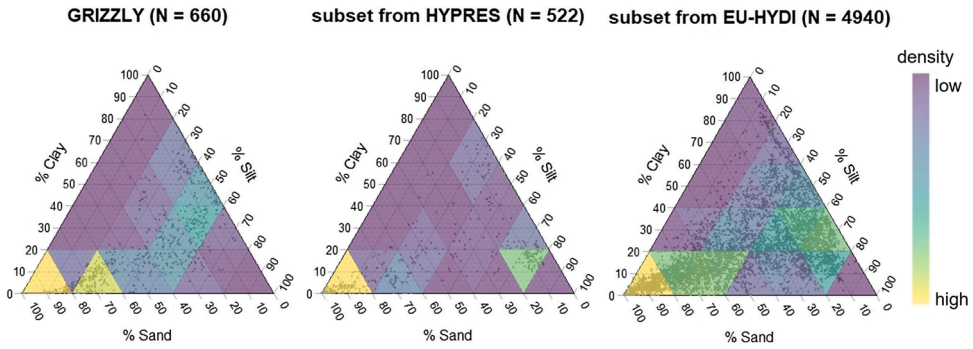

Fig. 1. Sand, silt, and clay content of the three datasets (GRIZZLY, HYPRES, and EU-HYDI) used to analyze the performance of the PTFs. The density of the data in the cells is indicated with the colorbar spanning from high (yellow) to low (blue) values.

incomplete data from our analysis. Therefore, a total of 6122 data for WRF were obtained from the three databases, consisting of measured soil bulk density, ρ_b (g cm^{-3}), percentages of clay, silt, and sand contents (%), soil organic carbon content (in percent), laboratory-measured water retention data, $\theta_{OBS}(\psi)$ including saturated water content, and θ_s (cm^3 cm^{-3}). Fig. 1 shows the distribution of soil samples of the three datasets in the texture triangle.

Three soil hydraulic parameters (θ_r, α, n) featuring in the vG WRF were optimized by interpolating the vG equation (Eq. (1)) on observed soil water content and matric head data pairs. For the prediction of saturated hydraulic conductivity, K_s (cm d^{-1}), 62 soil samples out of 660 were selected in GRIZZLY, 253 soil samples out of 522 were selected in HYPRES, and 1811 of 14182 soil samples were selected in EU-HYDI. Therefore, a total of 2126 soil samples were used to evaluate prediction performance to estimate K_s.

2.3. Evaluation criteria

The most common metrics used to quantify the predictive capability of the tested PTFs are: root mean square error (RMSE), which combines both bias and lack of precision, the coefficient of determination (R^2), which measures how well the data pairs fit a straight line, and the mean relative error (MRE), which quantifies the average under-estimation (if positive) or over-estimation (if negative). These statistical indicators are defined as follows:

$$RMSE = \sqrt{\frac{1}{N}\sum_{i=1}^{N}(O_i - P_i)^2} \tag{7}$$

$$R^2 = \frac{\sum_{i=1}^{N}(O_i - P_i)^2}{\sum_{i=1}^{N}\left(O_i - \overline{O_i}\right)^2} \tag{8}$$

$$MRE = \frac{1}{N}\sum_{i=1}^{N}\left(1 - \frac{P_i}{O_i}\right)\cdot 100 \tag{9}$$

where O, $\overline{O}$, and P are the observed, mean of observed, and predicted values of a variable, respectively. Subscript i is the counter and N is the highest number of counter-points. We specify that also the relative error (RE), namely RE = 1-P_i/O_i, was used in the data analysis.

The prediction performance on the WRF was also evaluated by using the integral mean deviation (IMD) which reveals biases in predicting the shape of the observed curve (IMD > 0 means systematic underprediction):

$$IMD = \frac{1}{(\xi_u - \xi_l)}\int_{\xi_l}^{\xi_u}[\theta(\xi)_{OBS} - \theta(\xi)_{PTF}]d\xi \tag{10}$$

where $\xi = \ln(\psi)$, with "ln" denoting the natural logarithm, whereas the subscripts u and l denote the upper and lower bounds, respectively. We set the prefixed lower and upper matric head values at 10° cm and $10^{4.2}$ cm, respectively, to cover the water retention curve from saturation up to the wilting point.

The Akaike information criterion (AIC) estimates the amount of information lost by a PTF and quantifies the trade-off between goodness of fit and model parsimony (Diks and Vrugt, 2010). The AIC is computed as follows:

$$AIC = lnNS\, ln\left(\frac{SSE}{NS-1}\right) + lnNS + 2p \tag{11}$$

where *NS* is the number of soil samples, *p* is the number of predictors employed in a PTF, and SSE is the sum of squared errors, given by:

$$SSE = \sum_{i}^{NS} (O_i - P_i)^2 \tag{12}$$

Statistical analysis was performed in MATLAB and R [version 4.0.3] (R Core Team, 2020).

For an optimal prediction, RMSE, MRE, and IMD should be close to zero, R^2 values should be close to 1 whereas AIC should be as high as possible (Romano and Palladino, 2002; De Vos et al., 2005). The RMSE is widely used in the body of scientific literature and generally spans between 0.020 and 0.12 $cm^3\ cm^{-3}$, expressing very high and very low performances, respectively (Schaap et al., 2001; Cornelis et al., 2001; Sing et al., 2020). Ideally, perfect performance is obtained when all individual MRE and IMDs are zero, while in reality underestimation and overestimation are obtained when MRE and IMD values are positive or negative, respectively. The AIC penalizes PTFs using a large number of predictors and indicates that model complexity is not always associated with high performance.

2.4. Functional performance #1: impact of PTFs on assessing the spatial variability of soil-water content at field capacity

A functional performance analysis was carried out using the data collected in a small experimental catchment, called MFC1, located near the village of Monteforte Cilento in southern Italy (Nasta et al., 2019). MFC1 has a drainage area of approximately 5.0 ha and belongs to the Upper Alento River Catchment (Romano et al., 2018). Both disturbed soil samples and undisturbed soil cores were collected near the soil surface (vertical sampling at a soil depth of 10−17 cm) in 44 positions over a regular 25 m × 25 m sampling grid (see Fig. 1 in Nasta et al., 2019). Particle-size distribution, oven-dry soil bulk density, saturated soil water content, and saturated soil hydraulic conductivity were all determined by using standard laboratory methods (Mebius, 1960; Gee and Or, 2002; Topp and Ferré, 2002; Reynolds and Elrick, 2002). For each soil core, the vG-equation (Eq. (1)) was fitted on soil water content and matric head data pairs that were measured by using suction tables and pressure plates (Romano et al., 2002).

Geostatistics was used to assess the capability of a PTF in quantifying the spatial variability of field capacity that is a key parameter depending on water retention characteristics. Based on the intrinsic hypothesis, the spatial variation of the target variable is quantified by a semi-variogram which is the square of the increments of θ_{FC} separated by a lag-distance *h*:

$$\gamma(h) = \frac{1}{2N(h)} \sum_{i=1}^{N(h)} [\theta_{FC}(x_i) - \theta_{FC}(x_i + h)]^2 \tag{13}$$

where $\gamma(h)$ is the experimental semi-variance, $N(h)$ is the number of pairs of observations separated by *h*, and x_i is the location of the *i*th observation. The semi-variances of the measured and predicted field capacity values were fitted to the Gaussian model proposed by Wackernagel (2003):

$$\gamma(h) = c\left[1 - exp\left(-\frac{h^{1.5}}{r^{1.5}}\right)\right] \tag{14}$$

where *c* is the sill and *r* is a distance parameter. This Gaussian model approaches the sill asymptotically, but a practical range can be approximated as $\sqrt{3}\ r$ when the variogram reaches about 95 % of the sill.

The best-performing PTFs were selected from the results of the regional-scale evaluation presented in Section 3.1. In this functional evaluation, the objective is to evaluate the ability of the PTFs to describe the spatial variability of field capacity (θ_{FC}) values. We used the ordinary kriging method to generate spatial interpolation maps of the observed and PTF-predicted θ_{FC} values at unvisited locations over the study area (MFC1). Performance is assessed by considering the RMSE values (Eq. (7)) and R^2 (Eq. (8)). If not mentioned otherwise, all calculations were performed using MATLAB scripts.

2.5. Functional performance #2: impact of PTFs on water balance components simulated in Hydrus-1D

We quantify the epistemic uncertainty arising when soil water dynamics is described by a Richards-based model that is parameterized by either observed or PTF-predicted soil hydraulic parameters. We used Hydrus-1D (Šimůnek et al., 2018) with the same model set-up presented in Romano and Nasta (2016). Hydrus-1D solves numerically the following one-dimensional Richards equation for variably saturated soil water flow:

$$\frac{\partial \theta}{\partial t} = \frac{\partial}{\partial z}\left[K(\psi)\left(\frac{\partial \psi}{\partial z} + 1\right)\right] - \xi(z, \psi, T_p) \tag{15}$$

where *t* is time, *z* is a vertical coordinate taken positive upward, ψ is matric head, θ is the soil volumetric water content, and $\zeta(z,\psi,T_p)$ is the volumetric sink term function that describes macroscopic root water uptake.

Briefly, the study area is located near Acerra, a town belonging to the province of Naples (southern Italy) where the soil is classified as a typical Andosol of Vesuvius origin and land use was a peach orchard. A total of 89 undisturbed soil cores were collected along a transect at equal distances of 150 cm and a soil depth of 40 cm. Previous investigations in this area showed that the soil is well-drained, with a very deep groundwater table, and the soil hydraulic properties can be assumed as quite uniform up to a soil depth of approximately 90 cm (Romano, 1993; Ciollaro and Romano, 1995). Thirteen years (2000–2012) of weather data – for a total of 4749

Table 3
Performance of PTFs predicting soil water content at 30 prescribed matric head values in GRIZZLY (660 soil samples), HYPRES (522 soil samples) and EU-HYDI (4940 soil samples). NS: total number of soil samples; p = number of predictors; RMSE: root mean square error; R^2: coefficient of determination; IMD_a: average integral mean deviation; AIC: Akaike information criterion. Text in italics indicates when a part of or the entire data set was used to train the PTF.

PTF	*p*	GRIZZLY (NS = 660)				HYPRES (NS = 522)				EU-HYDI (NS = 4940)			
		RMSE $cm^3\ cm^{-3}$	R^2	IMD_a $cm^3\ cm^{-3}$	AIC	RMSE $cm^3\ cm^{-3}$	R^2	IMD_a $cm^3\ cm^{-3}$	AIC	RMSE $cm^3\ cm^{-3}$	R^2	IMD_a $cm^3\ cm^{-3}$	AIC
SAX86	2	0.111	0.72	0.470	−18.0	0.146	0.57	0.457	−13.8	0.120	0.57	0.4528	−23.6
C&S92	3	0.148	0.43		−12.3	0.146	0.44		−11.8	0.059	0.51		−33.6
R&B85	3	0.071	0.87	0.333	−21.9	0.083	0.84	0.296	−18.9	0.059	0.76	0.3275	−33.6
O&C80	4	0.146	0.52	0.472	−10.5	0.174	0.37	0.465	−7.6	0.146	0.43	0.4502	−16.3
WOS99	5	0.056	0.91	0.048	−20.9	*0.066*	*0.89*	*0.040*	*−17.7*	0.060	0.85	0.0082	−29.3
VER89	4	0.088	0.81	0.336	−17.1	0.094	0.81	0.333	−15.3	0.080	0.78	0.3774	−26.4
euptfv2	6	0.079	0.80	0.080	−14.4	0.071	0.87	0.058	−14.9	*0.045*	*0.91*	*0.0207*	*−32.2*
WEY09	4	0.046	0.91	0.002	−25.4	0.061	0.88	−0.003	−20.7	0.069	0.80	−0.0332	−29.0
ROSETTA	4	0.102	0.80	0.135	−15.2	0.104	0.81	0.118	−14.0	0.094	0.75	0.0983	−23.8
T&H98	3	0.082	0.81		−20.0	0.126	0.63		−13.7	0.110	0.61		−23.1
RAW82	5	0.067	0.84		−18.6	0.077	0.79		−15.9	0.082	0.68		−24.0

daily values – were acquired by an automated weather station located near the experimental field. The crop-specific potential evapotranspiration, ET_p, is computed from the meteorological data and partitioned into potential evaporation, E_p (cm d^{-1}), and potential transpiration, T_p (cm d^{-1}). Precipitation, P, and potential evapotranspiration, E_p, are system-dependent upper boundary conditions, whereas T_p determines the potential root water uptake. Both E_p and T_p are reduced by water limitation and stresses to actual evaporation (E_a) and actual transpiration (T_a).

Hydrus-1D was run in each of the 89 positions along the transect by using the 4749 daily values (13-year-long time series) of rainfall and potential evapotranspiration while setting a free-drainage lower boundary condition at 200 cm soil depth. The maximum rooting depth of the peach trees was assumed to be 80 cm. We built a set of numerical simulations depending on measured and predicted soil hydraulic vG-parameters with PTFs selected from the results of the regional-scale evaluation presented in Section 3.1. The following four water balance components are considered: water storage, WS_d, actual evaporation, $E_{a,d}$, actual transpiration, $T_{a,d}$, and drainage flux at the soil depth of 200 cm (soil profile bottom), Q_d, at a daily time step (indicated by subscript d). The abovementioned spatial-average daily fluxes were aggregated in annual sums. A total of 13 spatial-average annual sums were obtained in the transect of the 89 positions, thereby generating the spatial-average annual mean sums of $E_{a,y}$, $T_{a,y}$, and Q_y (indicated by subscript y).

The daily water storage values based on observed and PTF-estimated soil hydraulic properties were compared by using RMSE (Eq. (7)) and R^2 (Eq. (8)). The MRE_{WS} (Eq. (9)) in terms of daily water storage is calculated to quantify the model output discrepancy derived from the use of observed and PTF-estimated soil hydraulic properties. Similarly, the relative error (RE) in terms of field capacity (RE_{FC}) and saturated hydraulic conductivity (RE_{Ks}, transformed in $\log_{10}$ values) is considered to indicate the difference between direct observations and estimations.

3. Results and discussion

3.1. Regional-scale evaluation using the GRIZZLY, HYPRES, and EU-HYDI databases

3.1.1. Estimation of water retention function

The eleven PTFs listed in Table 1 were used to estimate the soil water content value (θ_{PTF}) at fixed matric heads ($N = 30$) with a regular step between 10° cm (i.e. very close to full saturation) and $10^{4.2}$ cm (i.e. at the conventional permanent wilting point, PWP).

The performance indicators (RMSE, R^2, IMD_a, AIC) listed in Table 3 show substantially different performances of the tested PTFs when using the three datasets (GRIZZLY, HYPRES, and EU-HYDI). The IMD_a values reported in Table 3 represent the average values of individual IMDs. The IMD index depends on the shape of the water retention function (Minasny and McBratney, 2003). IMD values could not be calculated for C&S92, T&H98, and RAW82. Most of the PTF estimates show an underestimation tendency, as indicated by the positive IMD values in Table 3.

Based on the RMSE values (Table 3), the vG-based PTFs outperform the others although the European PTFs (WEY09, VER89, euptfv2, WOS99) were trained on soil samples extracted from the GRIZZLY, HYPRES, and EU-HYDI databases. This regional analysis does not provide information about the validation of the PTFs but gives a general overview of their performance on large European datasets and suggests a pre-selection of a smaller set of PTFs available in the literature. The AIC indicates a high risk of overfitting when including soil bulk density and organic matter content as predictors without gaining accuracy (Table 3). Those PTFs omitting organic matter and bulk density as predictors obtained lower RMSE, better IMD, and higher R^2 values. Indeed, the soil organic carbon content and oven-dry bulk density are time-variant properties as affected by agricultural practices and environmental conditions, and very often show seasonal effects. Therefore, their impact on the soil hydraulic properties can be cumbersome. By isolating the relationship between soil texture and PTF accuracy, it is possible to find room for potential improvement. Fig. 2 graphically illustrates the RMSE values distributed in the USDA (United States Department of Agriculture) soil texture triangle when using four PTFs (SAX86, VER89,

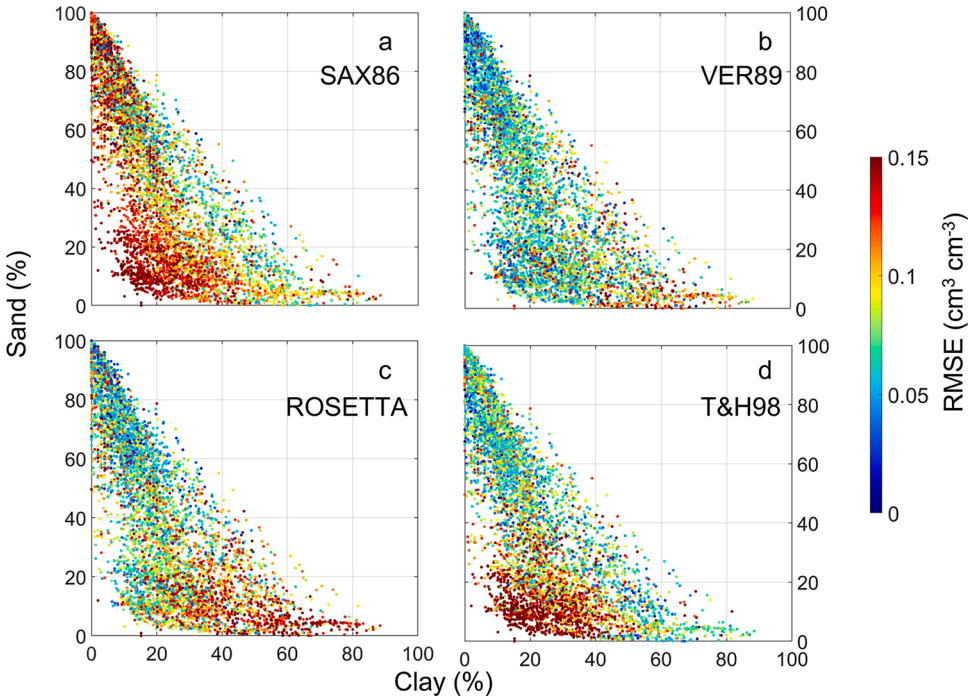

Fig. 2. RMSE values distributed in the USDA soil texture triangle by using a) SAX86, b) VER89, c) ROSETTA, d) T&H98. The total number of soil samples is 6122 (GRIZZLY, HYPRES, EU-HYDI databases).

Table 4
Performance of ten PTFs predicting $\log_{10}(K_s)$ in GRIZZLY (62 soil samples), HYPRES (253 soil samples), and EU-HYDI (1811 soil samples). NS: total number of soil samples; p = number of predictors; RMSE: root mean square error; R^2: coefficient of determination; AIC: Akaike information criterion. Text in italics indicates when a part of or the entire data set was used to train the PTF.

		GRIZZLY (NS = 62)			HYPRES (NS = 253)			EU-HYDI (NS = 1811)		
PTF	*p*	RMSE $cm^3\ cm^{-3}$	R^2	AIC	RMSE $cm^3\ cm^{-3}$	R^2	AIC	RMSE $cm^3\ cm^{-3}$	R^2	AIC
WOS99	5	1.350	0.28	16.67	*1.666*	*0.04*	*21.20*	1.686	0.078	25.34
euptfv2	6	1.347	0.02	18.65	1.120	0.14	18.81	*0.793*	*0.711*	*16.02*
ROSETTA	4	1.625	0.24	16.20	1.918	0.02	20.76	1.768	0.064	24.06
A&G19	5	1.145	0.24	15.31	1.732	0.13	21.63	1.685	0.019	25.33
GUP20	3	1.409	0.36	13.03	1.851	0.03	18.37	1.769	0.014	22.07
COS84	2	1.329	0.40	10.54	1.803	0.13	16.08	1.787	0.035	20.21
S&R06	3	1.437	0.26	13.19	1.891	0.07	18.60	1.811	0.006	22.42
VER89& GUA07	4	2.574	0.18	20.00	1.814	0.08	20.15	2.229	0.067	27.53
R&B85& NAS13	3	1.286	0.39	12.27	2.144	0.11	20.00	1.943	0.063	23.47
WEY09& GUA07	4	1.057	0.27	12.65	1.404	0.15	17.31	1.458	0.037	21.16

ROSETTA, T&H98). High RMSE values cluster in specific texture classes.

For example, VER89 (Fig. 2b) and ROSETTA (Fig. 2c) were calibrated on coarser-textured soil samples and consequently provided relatively high RMSE for the finer soil textural classes (Vereecken et al., 1989; Zhang and Schaap, 2019). The particle-size distributions of the soil samples depicted in Fig. 2 in Tomasella and Hodnett (1998) and Fig. 1 in Saxton et al. (1986) are also very different from those shown in Fig. 4a and d, respectively. T&H98 is less accurate when soil texture is silty or loamy, whereas SAX86 (based only on clay and sand contents as predictors) has room for improvement overall of the soil textural classes. SAX86, ROSETTA, and T&H98 were developed by using soil samples collected outside Europe (USA and Brazil), whereas VER89 was implemented by using a relatively small number of soil samples collected in Belgium. Therefore, these PTFs can be potentially re-calibrated in GRIZZLY, HYPRES, and EU-HYDI databases and further improved. A fairly uniform distribution of high RMSE (mostly reddish circles) values is observed for C&S92 and O&C80 (not shown), while the uniform distribution of low RMSE (mostly bluish circles) values is reported for R&B85, WOS99, euptfv2, WEY09, and RAW82 (not shown).

3.1.2. Estimation of saturated hydraulic conductivity

The ten PTFs listed in Table 2 were used to estimate saturated hydraulic conductivity by using 62, 523, and 1811 soil samples in

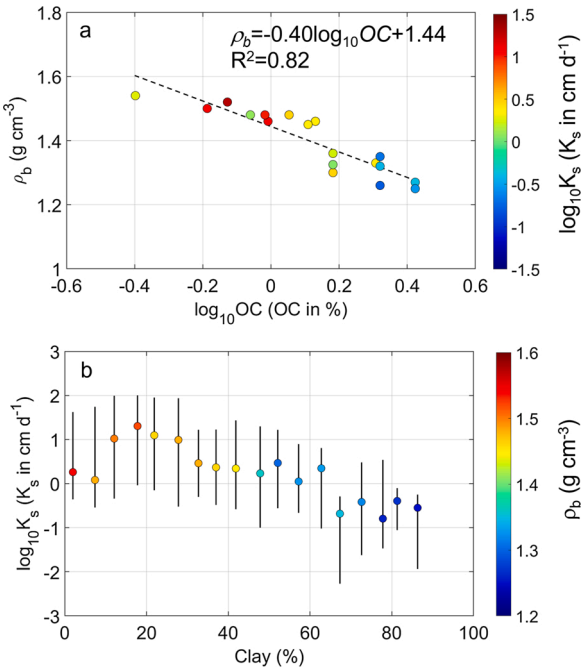

Fig. 3. Relationship between a) median organic content, *OC* (in decimal logarithmic values) and median soil bulk density, ρ_b (circles are colored according to median K_s data, expressed in decimal logarithmic values) calculated in each 5% clay class, b) 5% clay classes and median $\log_{10}K_s$ (circles are colored according to the median ρ_b) (NS = 2126). Vertical bars indicate 25th and 75th percentiles of $\log_{10}K_s$.

GRIZZLY, HYPRES, and EU-HYDI, respectively (total NS = 2126). The performance – in terms of RMSE and R^2 and AIC – of the ten PTFs in the three data sets for predicting the $\log_{10}K_s$-values is listed in Table 4.

All of the tested PTFs provide RMSE values systematically greater than 1 (i.e. greater than at least one order of magnitude), and R^2 values lower than 0.40. Similarly, as mentioned in Section 3.1.1, this analysis provides information about general regional performance: PTFs trained on all or part of GRIZZLY, HYPRES, or EU-HYDI performed better as a matter of course. Small homogeneous data sets (GRIZZLY) tend to provide better error metrics than data-rich databases (EU-HYDI). K_s depends on soil structural properties especially in the uppermost soil horizons (soil depth of soil samples in UARC refers to 10−17 cm).

Validation of site-specific calibrated PTFs usually leads to RMSE values spanning between 0.4 and 1.49 and R^2 values between 0.15 and 0.87 (see Table 3 in Zhang and Schaap, 2019). A positive exception is WEY09, which takes on lower-than-expected AIC-values when compared with other PTFs using the same number of predictors ($p = 4$).

Those PTFs taking advantage of the knowledge of WRF parameters to derive K_s (Guarracino, 2007; Nasta et al., 2013) are useful only if these retention parameters are fairly determined. This suggests that the availability of the WRF is precious information when one would guess a K_s value within a prediction uncertainty of a few orders of magnitude, whereas soil physical and chemical attributes have a poor prediction power to infer K_s satisfactorily. Minasny and Hartemink (2011) suggested that the PTF performance depends on data quality rather than PTF complexity. In EU-HYDI, the K_s values were obtained using several laboratory or *in situ* techniques; the soil sample sizes used for the measurement also vary greatly.

Saturated hydraulic conductivity, K_s, is the scale parameter for the hydraulic conductivity function (see Eq. (4)) and presents the drawback of varying over several orders of magnitude when soil matric heads ($|\psi|$ in cm) span from full saturation ($|\psi| = 0$) to extreme dryness ($\log_{10}|\psi|$ about 7). Numerous empirical data-driven analyses found that the intertwining controlling factors in determining K_s are soil texture, oven-dry soil bulk density, and soil organic carbon content. As a general statement, it is well-known that K_s decreases as the clay content increases, with increasing oven-dry soil bulk density (related to soil porosity in Eq. (2)). Instead, oven-dry soil bulk density is inversely related to soil organic carbon content (Zhang and Schaap, 2019). The analytical relationships calculating K_s from water retention parameters (see Eqs. (5) and (6)) evidence this assumption by posing K_s directly proportional to θ_s (close to soil porosity) and inversely proportional to the square of bubbling matric head which, in turn, indirectly depends on soil texture (Poiseuille's law). As it is quite difficult to find empirical relations by using the original data set, we group data into 5% clay classes (0–5 %, 5–10 %, and so on) and calculate median values of bulk density, $\log_{10}OC$, and $\log_{10}K_s$ (after testing normality of their statistical distribution, not shown) in each clay class. The decreasing relation between $\log_{10}OC$ and oven-dry bulk density is quantified through an empirical regression function with a high R^2-value (Fig. 3a). The circles in Fig. 3a are colored according to $\log_{10}K_s$-values that corroborate published data analysis because most probable $\log_{10}K_s$-values occur when oven-dry soil bulk density is low and organic carbon content is high and tend to increase along the empirical regression line. Nonetheless, this is only a qualitative statement because K_s of soils varies over several orders of magnitude and is affected by unpredictable controlling factors. Another qualitative assessment can be drawn by a visual inspection of Fig. 3b that relates 5% clay content classes and median $\log_{10}K_s$-values (the vertical bars indicate

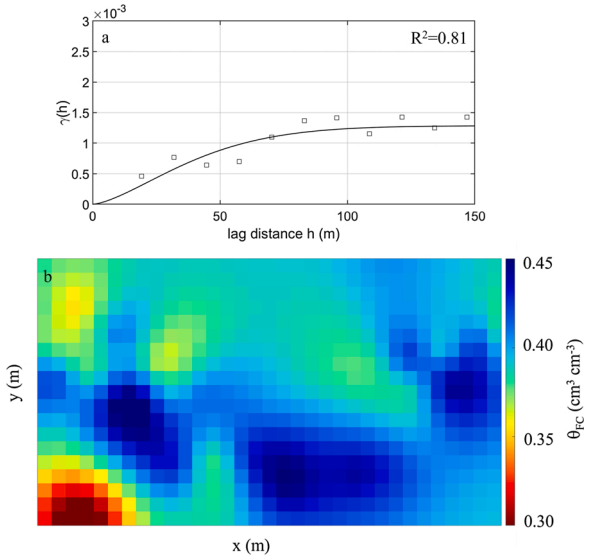

Fig. 4. a) Gaussian model function fitted on the isotropic experimental variograms and b) map of interpolated field capacity (θ_{FC}) values by using the ordinary kriging based on measured field capacity data (NS = 44).

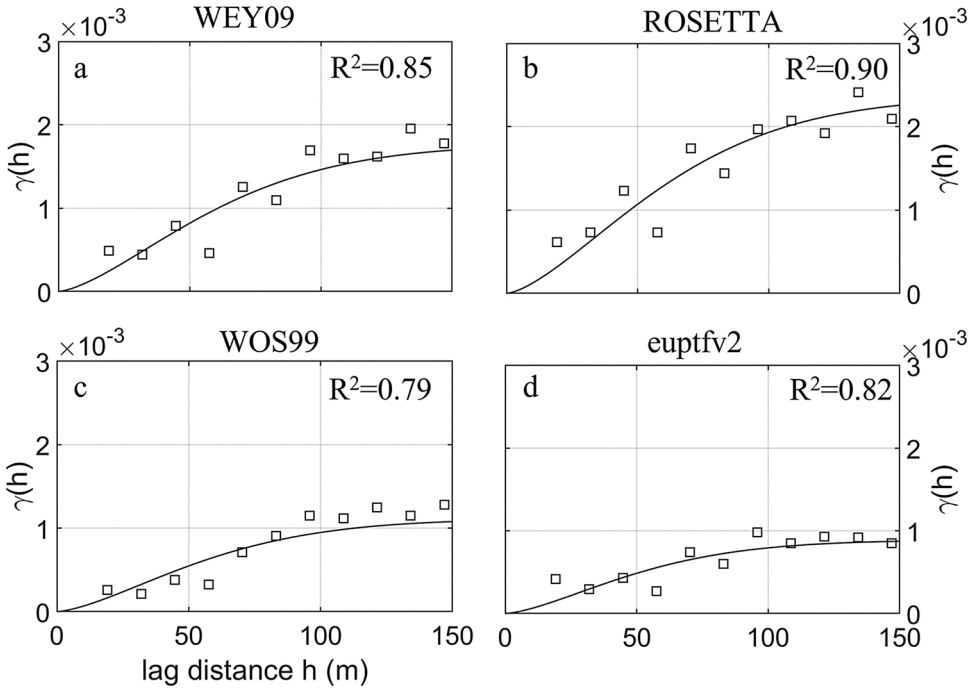

Fig. 5. Gaussian model functions fitted on the isotropic experimental variograms based on PTF-predicted field capacity data, a) WEY09, b) ROSETTA, c) WOS99, d) euptfv2. The goodness of fit is also quantified by R^2 values reported in each subplot.

25th and 75th percentiles). It is expected that $\log_{10}K_s$-values should linearly decrease with increasing clay content. This is observed by a decreasing trend with low $\log_{10}K_s$-values for very high clay content. However, the trend line is balanced by the contrasting impact of soil bulk density (circles in Fig. 3b are colored according to soil bulk density) that can be considered a crude proxy of soil structure. The effect of other unquantifiable controlling factors adds jeopardy and makes the prediction of K_s very problematic and rather cumbersome (Eck et al., 2016; Ilek et al., 2019).

In this section, four vG-based PTFs (namely WEY09, ROSETTA, euptfv2, and WOS99) outperformed the others and are therefore selected for the functional evaluation presented in the relevant sections below.

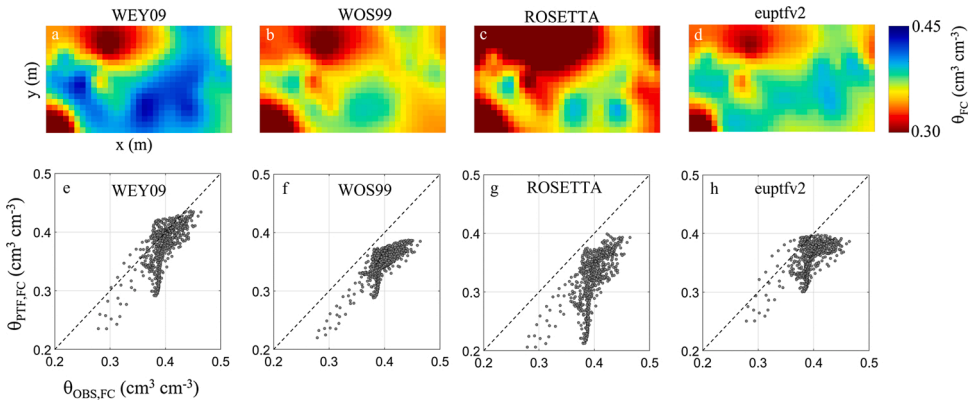

Fig. 6. Map of interpolated field capacity (θ_{FC}) values by using the ordinary kriging based on a) WEY09, b) WOS99, c) ROSETTA, d) euptfv2; comparison between observed ($\theta_{OBS,FC}$) and estimated ($\theta_{PTF,FC}$) field capacity values obtained by kriging based on e) WEY09, f) WOS99, g) ROSETTA, h) euptfv2.

Table 5
Coefficient of determination (R^2) and root mean squared error (RMSE) between observed and PTF-estimated field capacity values over the 44 positions (parametric evaluation) and maps interpolated by ordinary kriging (functional evaluation).

	parametric evaluation		functional evaluation	
	R^2	RMSE $cm^3\ cm^{-3}$	R^2	RMSE $cm^3\ cm^{-3}$
WEY09	0.568	0.0287	0.492	0.0334
WOS99	0.728	0.0503	0.632	0.0533
ROSETTA	0.512	0.0716	0.428	0.0817
euptfv2	0.589	0.0415	0.491	0.0424

3.2. *Results of functional performance #1*

In this section, it is crudely hypothesized that 44 observations are able to fully describe the spatial variability of the soil water content values at "field capacity" in the study catchment. Although this relatively small number of available soil samples can be critical in spatial variability studies, we are aware that the majority of real-world case studies are based on a limited number of soil samples. The goal of this section is to evaluate the capability of four PTFs selected in the previous section to map the field capacity, θ_{FC}, values. Based on the general regional evaluation WEY09, ROSETTA, euptfv2, and WOS99 performed the best. In this case, it is important not only to quantify the accuracy at estimating field capacity but also the ability to reproduce the same observed spatial structure in a study area (MFC1). Spatial prediction provides estimates of field capacity values at unvisited locations. We used the ordinary kriging model to assess the spatial uncertainty arising when the error in predicting field capacity values propagates in unsampled locations. Fig. 4 a shows the stable Gaussian model (Eq. (13)) fitted on the experimental isotropic variograms based on 44 measured field capacity data in MFC1. Fig. 4b illustrates the 10 m grid size (a total of 680 cells) interpolation of observed field capacity using ordinary kriging based on the spatial information described by the Gaussian model fitted on the observations.

The Gaussian model was fitted also to the isotropic variograms computed using the four PTF-predicted field capacity data (Fig. 5). The goodness of fit was quantified in terms of R^2-values (Eq. (8)). Fig. 6 shows the maps of the PTF-estimated field capacity values interpolated by ordinary kriging (top panel in Fig. 6; WEY09, WOS99, ROSETTA, euptfv2 in Fig. 6a–d, respectively). The comparison between these observed and estimated data over the 680 cells of the study area is depicted in the bottom panel of Fig. 6 (WEY09, WOS99, ROSETTA, euptfv2 in Fig. 6e–h, respectively).

The RMSE values, as well as R^2 values reported in Table 5, are used for evaluating prediction performance over the 44 measurement positions (parametric evaluation) and the 680 cells (functional evaluation). In the parametric evaluation, the RMSE values are very low for WEY09, acceptable for euptfv2, WOS99, and high for ROSETTA. In the functional evaluation, the quality of the ordinary kriging deteriorates (especially for WEY09 and ROSETTA). RMSE values referring to the interpolated maps of field capacity (functional evaluation) are higher than the corresponding RMSE referring to field capacity values over the 44 positions (parametric evaluation) with increments spanning from 3% (euptfv2) up to 16 % (WEY09). These results are corroborated by the corresponding R^2 values in the functional evaluation that are worse (lower) than those reported in the parametric evaluation. Moreover, the PTF predictions clearly underestimate the observations as illustrated in Fig. 6 with highest bias observed for WOS99 and ROSETTA. The best PTFs are WEY09 and euptfv2 in terms of RMSE values. These results reflect the similar predictive performance reported on data in the three European databases (Table 3).

The interpolation of soil hydraulic properties at unvisited locations within the study area is strategic to properly implement

Table 6
Observed (OBS) and PTF-predicted spatial-average annual mean $E_{a,y}$, $T_{a,y}$, Q_y in Hydrus-1D.

	$T_{a,y}$ cm y^{-1}	$E_{a,y}$ cm y^{-1}	Q_y cm y^{-1}
OBS	53.16	31.71	−4.74
WEY09	52.57	30.52	−6.92
WOS99	54.69	30.73	−5.00
ROSETTA	54.55	33.50	−2.83
euptfv2	53.71	30.44	−6.02

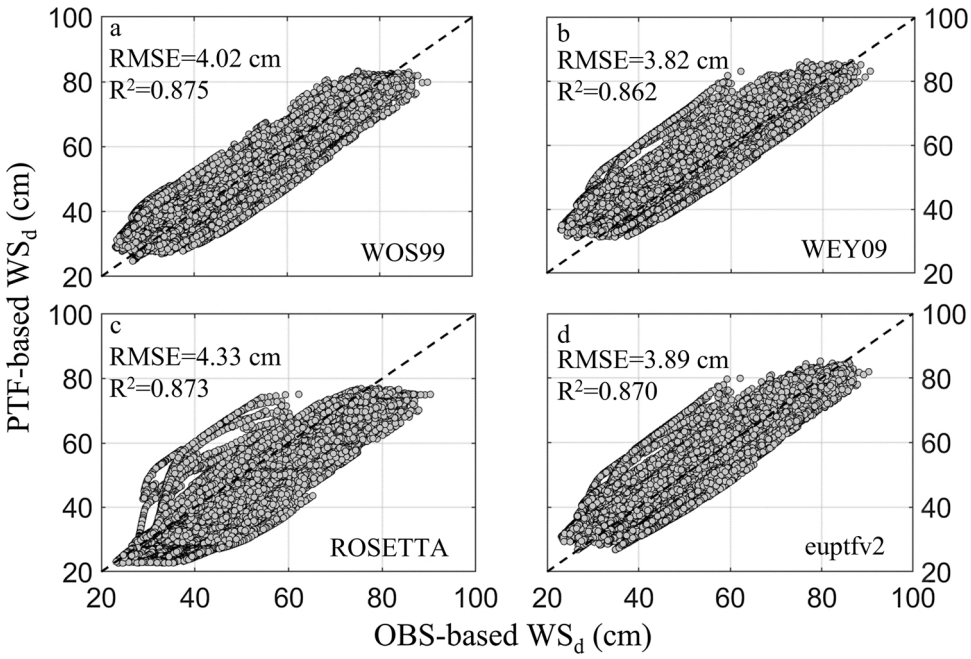

Fig. 7. Comparison between observed (OBS-based WS_d) and estimated (PTF-based WS_d) water storage data based on a) WOS99, b) WEY09, c) ROSETTA, d) euptfv2. Performance is evaluated in terms of RMSE and R^2 reported in each subplot.

distributed water balance models. Deviations from actual values of a spatial-dependent variable estimated by a simplified procedure can have little effect on the calculation of the mean value in a certain area. In contrast, the distribution in space of the estimated values of the target variable can differ from that of the actual values to alter the patterns of the semi-variograms significantly. Romano and Santini (1997) compared the variograms fitted on observed water retention data with the predictions generated by four published PTFs. They used a spherical model to fit the experimental semi-variograms of soil water content at the fixed matric head values. The same authors (1997) selected VER89 as the best PTF to predict the spatial variability of the water retention function. They concluded that the observed discrepancy in structural information can be considered a penalty to be paid when using a simplified methodology to obtain a large number of soil hydraulic parameter values. Few studies have investigated whether PTFs reliably describe spatial variability of soil hydraulic properties in the field (Liao et al., 2011; Silva et al., 2017). Romano (2004) investigated the ability of a PTF to provide a picture of the actual spatial variations exhibited by a soil attribute and, more importantly, emphasized the fact that when using a PTF one should consider two additional issues: *i*) the scale (an issue that strongly interacts with the concept of spatial variability; see Pringle et al., 2007) and *ii*) the ultimate goal of obtaining effective parameters to be employed in a governing equation of motion.

In the case of mapping soil hydraulic properties in the catchment of Lake Balaton, there was no significant difference in performance between PTF-based and geostatistical maps when environmental properties – e.g.: topography, climate, vegetation – were considered among the predictors alongside basic soil properties. However, locally extreme values can be better described when residual kriging is added (Szabó et al., 2019b).

3.3. Results of functional performance #2

This section addresses the question of how and to what extent the epistemic errors that arise from improper use of PTF-predicted soil hydraulic parameterization propagate when an annual soil water budget is simulated at the field scale. Mean annual precipitation (P_y) and potential evapotranspiration ($ET_{p,y}$) are 90.13 cm y^{-1} and 172.37 cm y^{-1}, respectively. As in the previous section, we used the

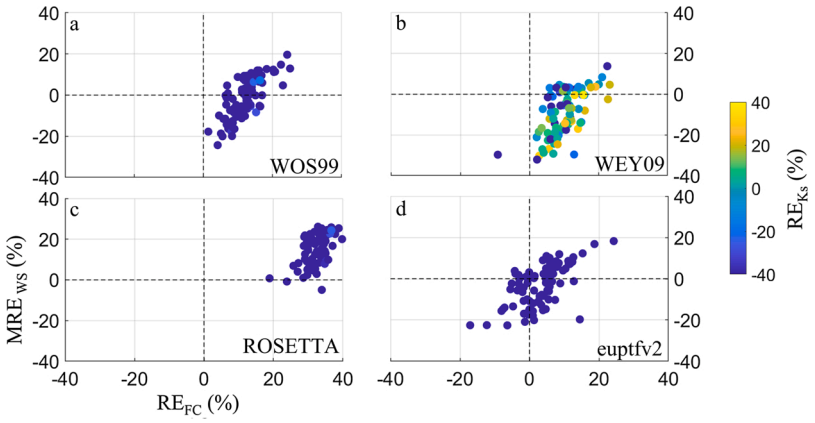

Fig. 8. Relationship between relative error in terms of field capacity (RE_{FC}) and mean relative error in terms of water storage when using observed and predicted soil hydraulic parameters. PTFs are: a) WOS99; b) WEY09; c) ROSETTA and d) euptfv2. Circles are colored according to the relative error in terms of saturated hydraulic conductivity (RE_{Ks}) expressed in $\log_{10}$ values.

Table A1
Tabulated regression coefficients (*a*, *b*, *c*, *d*) in Eq. (A22) to predict soil water content values associated to nine prescribed matric head values.

ψ	*a*	*b*	*c*	*d*
cm				
−1	2.24	0.298	0.159	37.937
−10	0	0.530	0.255	23.839
−30	0	0.552	0.262	18.495
−60	0	0.576	0.300	12.333
−100	0	0.543	0.321	9.806
−330	0	0.426	0.404	4.046
−1,000	0	0.369	0.351	3.198
−5,000	0	0.258	0.361	1.567
−15,000	0	0.150	0.396	0.910

Table A2
Tabulated regression coefficients (*a*, *b*, *c*, *d*, *e*, *f*) in Eq. (A23) to predict soil water content values associated with 12 prescribed matric head values.

ψ	*a*	*b*	*c*	*d*	*e*	*f*
cm						
−40	0.7899	−0.0037	0	0	0.0100	−0.1315
−70	0.7135	−0.0030	0	0.0017	0	−0.1693
−100	0.4118	−0.0030	0	0.0023	0.0317	0
−200	0.3121	−0.0024	0	0.0032	0.0314	0
−330	0.2576	−0.0020	0	0.0036	0.0299	0
−600	0.2065	−0.0016	0	0.0040	0.0275	0
−1,000	0.0349	0	0.0014	0.0055	0.0251	0
−2,000	0.0281	0	0.0011	0.0054	0.020	0
−4,000	0.0238	0	0.0008	0.0052	0.0190	0
−7,000	0.0216	0	0.0006	0.0050	0.0167	0
−10,000	0.0205	0	0.0005	0.0049	0.0154	0
−15,000	0.0260	0	0	0.0050	0.0158	0

four PTFs (namely WEY09, ROSETTA, euptfv2, and WOS99) selected in Section 3.1 to estimate the soil hydraulic parameters over the 89 positions along the experimental transect. Table 6 shows the spatial average mean annual $E_{a,y}$, $T_{a,y}$, Q_y of the observed and PTF-estimated 5 sets (namely OBS, WEY09, ROSETTA, euptfv2, and WOS99) of numerical simulations relying on 4749 daily values in the 89 positions. When considering the numerical simulations controlled by observed soil hydraulic properties, the mean annual actual evapotranspiration ($ET_{a,y}$) is 84.87 cm which represents about 94 % and 49 % of P_y and $ET_{p,y}$, respectively. $T_{a,y}$ is the dominant flux representing about two-thirds of $ET_{a,y}$. Q_y represents about 5% of P_y while surface runoff is negligible. The use of soil hydraulic properties predicted by the four PTFs leads to water balance components being different from those obtained by simulations based on direct observations (Table 6). WOS99 outperforms the other PTFs, obtaining $ET_{a,y}$ and Q_y values with errors lower than 1 cm per year. ROSETTA is the worst-performing PTF in this exercise.

The differences reported in terms of annual water balance components ($E_{a,y}$, $T_{a,y}$, Q_y) in Table 6 are reflected in terms of total daily

water storage values (total number of 422661 values is given by 4749 days multiplied by 89 positions). The relationship (Fig. 7) between a total of 422661 water storage data based on observed soil hydraulic properties and water storage data based on PTF-estimated soil hydraulic properties is evaluated in terms of RMSE and R^2 for the four PTFs (WOS99, WEY09, ROSETTA, and euptfv2). The lowest RMSE is obtained by WEY09 while the highest R^2 is obtained by WOS99. ROSETTA tends to underpredict water storage data, WEY09 and euptfv2 tend to overpredict, while WOS99 obtains the least biased simulations of water storage values. Yet it is still not possible to determine the best-performing PTF. Hence it is important to interpret and analyze the impact of soil parameterization on the daily water storage simulated in Hydrus-1D.

To this end, the differences between measured and predicted soil hydraulic parameters can be evaluated by using the relative error (RE) over the 89 positions in terms of the field capacity (RE_{FC}), and $\log_{10}K_s$(RE_{Ks}). On the other hand, we calculate the mean relative error (MRE_{WS}) from daily water storage values (WS_d) based on observed and predicted soil hydraulic parameters in each position of the experimental transect (Eq. (9)).

The impact of using the predicted soil hydraulic properties on the water balance simulated by Hydrus-1D is analyzed by relating the relative errors in terms of observed and predicted field capacity values (RE_{FC}), with MRE_{WS} depicted in Fig. 8. The circles are colored according to relative errors in terms of saturated hydraulic conductivity (RE_{Ks}). WOS99, WEY09, and ROSETTA consistently underestimate observed field capacity as indicated by positive biased values of RE_{FC} in Fig. 8. Importantly, ROSETTA leads to a relatively high RE_{FC}, ranging from 18.9% to 41.1%, whereas euptfv2 is the only PTF leading to a fairly unbiased RE_{FC}, ranging from –17.1 % and 24.3 % with a virtually zero mean value (RE_{FC} = 3.2 %). The parametric uncertainty propagates in the water balance computed by Hydrus-1D. The most accurate simulations of soil water storage values are based on WOS99 (MRE_{WS} ranging from –24.3 % and 19.6 % in Fig. 8a) and euptfv2 (MRE_{WS} ranging from –22.6 % and 18.3 % in Fig. 8d) as the corresponding MRE_{WS} values are centered around zero, which represents the ideal point on the y-axis. WEY09 (MRE ranging from –32.1 % and 13.8 % in Fig. 8b) and especially ROSETTA (MRE_{WS} ranging from –4.9 % and 30.4 % in Fig. 8c) are biased and their shifts bring about overestimation (mostly negative MRE_{WS} values) and underestimation (mostly positive MRE_{WS} values), respectively. The concept of precision is related to how much the sample data cluster among them and are quite close to their mean value; from a quantitative point of view, the standard deviation (or the variance, equivalently) indicates a good precision if its value is quite small. ROSETTA is the most precise PTF in terms of soil water storage with a standard deviation of 7.90 cm, partly because this indirect method is somewhat unable to reflect large parametric variability in the European data set. In contrast, WEY09 is the least precise PTF with a standard deviation of 10.93 cm. The strong positive relationships (Pearson correlation coefficients are 0.74, 0.71, 0.63, 0.67 for WOS99, WEY09, ROSETTA, and euptfv2, respectively) between RE_{FC} and MRE_{WS} indicate the high sensitivity of the numerical computations of soil-water storage to the water retention parameters employed to calculate the soil water content at field capacity (Eq. (3)). In other words, using PTF-predicted field capacity values higher than those obtained by direct observation leads to an overestimation in the simulated soil water storage. While euptfv2 outperforms the other PTFs in terms of field capacity estimates, it is clear that the lack of precision in guessing the soil water storage is due to a weak estimation of K_s-values (bluish circles in Fig. 8d). ROSETTA shows a significant bias in terms of both field capacity and K_s (bluish circles in Fig. 8c). WOS99 and WEY09 are characterized by similar relationships between RE_{FC} and MRE_{WS} (Fig. 8a and b). Nonetheless, WEY09 is the only PTF able to predict K_s reliably (with the majority of RE_{Ks} around zero, as indicated by the greenish circles in Fig. 8b).

Several studies present functional evaluations for water balance simulations, especially for comparing observed and estimated soil water content patterns (Nemes et al., 2003; Abkenar and Rasoulzadeh, 2019). Guber et al. (2009) performed a functional evaluation using Hydrus-1D to evaluate the impact on various components of the simulated water budget when parameterizing the Richards equation with 19 PTFs. Christiansen and Feyen (2001) found that the established saturated hydraulic conductivity and saturated water content were the most influential parameters in determining the uncertainty in the catchment-scale water budget. All these studies showed that parameterizing a hydrological model with PTF-predicted soil hydraulic properties is definitely a promising approach to overcome the issue of data scarcity.

4. Concluding remarks

The parametric evaluation of eleven PTFs to predict the water retention function and ten PTFs to predict the saturated hydraulic conductivity using a relatively large dataset collected over Europe enabled us to select the most accurate and reliable ones with respect to different spatial scales of interest. The most recent vG-based PTFs (WEY09, WOS99, euptfv2) proved to be accurate enough for predicting the water retention function. ROSETTA, VER89, SAX86, T&H98, and R&B85 performed acceptably and can be theoretically improved in some textural classes although they were calibrated and validated outside Europe under different climatic and environmental conditions.

The ten PTFs used to predict saturated hydraulic conductivity demonstrated a generally poor performance, with uncertainty spanning over one or two orders of magnitude. The main predictors (soil bulk density, organic carbon content, and texture) are cross-correlated and might play contrasting roles in predicting saturated hydraulic conductivity especially due to the lack of its standardized measurement method.

In this study, we evaluated the effectiveness of four vG-based PTFs – selected based on the outcomes of the parametric evaluations – to properly estimate the observed water contents at field capacity by considering a relatively small number of soil samples. Moreover, we also evaluated the ability of the PTFs to reproduce the kriged maps of field capacity, reporting a deterioration of prediction performance from 3% to 16 % in terms of RMSE values compared to parametric evaluation.

Finally, we evaluated the impact of parameterizing the Richards equation with PTF-predicted SHP on daily water fluxes as simulated by Hydrus-1D within a 2-m-thick uniform soil profile. We verified the hypothesis for which large discrepancies between

observed and PTF-predicted key soil hydraulic properties lead to substantial differences in simulated water fluxes. Although the four PTFs proved satisfactorily equivalent for simulating daily water storage values, we stress the importance of describing the sensitivity of model output to model parameterization.

Declaration of Competing Interest

The authors declare that they have no known competing financial interests or personal relationships that could have appeared to influence the work reported in this paper.

Acknowledgments

Contributions of P. Nasta and N. Romano were supported by the MiUR-PRIN Project "WATer mixing in the critical ZONe: observations and predictions under environmental changes – WATZON" (grant 2017SL7ABC). The authors would like to thank the European Commission and Netherlands Organisation for Scientific Research (NWO) for funding, in the framework of the collaborative international consortium (iAqueduct) financed under the 2018 Joint call of the Water Works 2017 ERA-NET Cofund. This ERA-NET is an integral part of the activities developed by the Water JPI (Project number: ENWWW.2018.5); Contribution of B. Szabó was supported by the János Bolyai Research Scholarship of the Hungarian Academy of Sciences (grant no. BO/00088/18/4) and European Union's Horizon 2020 research and innovation programme under grant agreement No. 862756, project OPTAIN.

Appendix A

Prediction of WRF parameters

We set 30 prescribed logarithmically spaced points between decades –10° cm and –$10^{4.176}$ cm of matric head, ψ, corresponding to ψ = –1 cm and ψ= –15,000 cm, respectively.

The equation proposed by Saxton et al. (1986) is the following:

$$\theta(\psi) = exp[ln(\psi/A)/B)] \tag{A1}$$

where *ln* is natural logarithm and

$$A = 100\ exp(-4.396 - 0.0715clay - 0.000488sand^2 - 0.00004285sand^2clay) \tag{A2}$$

$$B = -3.140 - 0.00222clay^2 - 0.00003484sand^2clay \tag{A3}$$

The equation proposed by Campbell and Shiozawa (1992) follows the analytical form of Brooks and Corey (1964):

$$\theta(\psi) = (\theta_s - \theta_r)\left(\frac{\psi_b}{\psi}\right)^{\lambda} + \theta_r \quad \text{for } \psi > \psi_b \tag{A4a}$$

$$\theta(\psi) = (\theta_s - \theta_r) + \theta_r \quad \text{for } \psi \le \psi_b \tag{A4b}$$

Matric head values, ψ, are obtained by setting 30 prescribed evenly spaced points of soil water content, θ between θ_s and θ_r. In this case $\theta_r = 0$:

$$\psi(\theta) = \psi_b(\theta/\theta_s)^{-\lambda} \tag{A5}$$

where:

$$\psi_b = \psi_{es}(\rho_b/1.3)^{0.67\lambda} \tag{A6}$$

$$\lambda = -20\psi_{es} + 0.2\sigma_g \tag{A7}$$

$$\psi_{es} = -0.05d_g^{-1/2} \tag{A8}$$

$$d_g = \exp(-0.025 - 0.0363silt - 0.0688clay) \tag{A9}$$

$$\sigma_g = \exp\left[0.133silt + 0.477clay - \left(lnd_g\right)^2\right]^{1/2} \tag{A10}$$

where ψ_{es} is the air entry matric head evaluated at a standard bulk density of 1.3 g cm^{-3}, σ_g is the geometric standard deviation, d_g geometric mean particle diameter.

Rawls and Brakensiek (1985) developed the following equations to estimate the Brooks and Corey parameters:

$$\psi_b = exp(5.3396738 + 0.185clay - 2.484por - 0.002clay^2 - 0.044sand\ por - 0.6175clay\ por + 0.0014sand^2por^2 - 0.009clay^2por^2 - 0.00002sand^2clay + 0.009clay^2por - 0.00072sand^2por + 0.0000054clay^2sand + 0.500por^2clay) \quad (A11)$$

$$\lambda = exp(-0.784 + 0.018sand - 1.062por - 0.00005sand^2 - 0.003clay^2 + 1.111por^2 - 0.031sand\ por + 0.0003sand^2por^2 - 0.0061clay^2por^2 - 0.00000235sand^2clay + 0.008clay^2por - 0.007por^2clay) \quad (A12)$$

$$\theta_r = -0.018 + 0.0009sand + 0.00513clay + 0.029por - 0.0002clay^2 - 0.001sand\ por - 0.0002clay^2por^2 + 0.0003clay^2por - 0.002por^2clay \quad (A13)$$

Soil porosity is computed from Eq. (2).

Oosterveld and Chang (1980) proposed the following equation:

$$\theta(\psi) = 0.01\rho_b\ (35.367 + 0.644clay - 0.251sand - 0.045D)\psi^{-0.19} \quad (A14)$$

where D is the mean depth of the sample expressed in units of cm.

Wösten et al. (1999) derived the parameters featuring in the van Genuchten equation (Eq. (1)):

$$\theta_s = 0.7919 + 0.001691clay - 0.29619\rho_b - 0.000001491silt^2 + 0.0000821OM^2 + 0.02427/clay + 0.01113/silt + 0.01472ln(silt) - 0.0000733\ OM\ clay - 0.000619\rho_b\ clay - 0.001183\rho_b\ OM - 0.0001664\ topsoil\ silt \quad (A15)$$

$$\alpha = exp(-14.96 + 0.03135clay + 0.0351silt + 0.646OM + 15.29\rho_b - 0.192topsoil - 4.671\rho_b^2 - 0.000781clay^2 - 0.00687OM^2 + 0.0449/OM + 0.0663ln(silt) + 0.1482ln(OM) - 0.04546\rho_b\ silt - 0.4852\rho_b\ OM + 0.00673topsoil\ clay) \quad (A16)$$

$$n = 1 + exp(-25.23 - 0.02195clay + 0.0074silt - 0.1940OM + 45.5\rho_b - 7.24\ \rho_b^2 + 0.0003658clay^2 + 0.002885OM^2 - 12.81/\rho_b - 0.1524/silt - 0.01958/OM - 0.2876ln(silt) - 0.0709ln(OM) - 44.6ln(\rho_b) - 0.02264\rho_b\ clay + 0.0896\rho_b\ OM + 0.00718topsoil\ clay) \quad (A17)$$

where $m = 1–1/n$ and $topsoil = 1$ (alternative value is zero if the PTF is applied for deeper soil layers).

Vereecken et al. (1989) derived the parameters featuring in the van Genuchten equation (Eq. (1)):

$$\theta_s = 0.81 - 0.283\rho_b + 0.001clay \quad (A18)$$

$$\theta_r = 0.015 + 0.005clay + 0.014OC \quad (A19)$$

$$\alpha = exp(-2.486 + 0.025sand - 0.351OC - 2.617\rho_b - 0.023clay) \quad (A20)$$

$$n = exp(0.053 - 0.009sand - 0.013clay + 0.00015sand^2) \quad (A21)$$

where $OC = OM/1.724$ and $m = 1$.

Tomasella and Hodnett (1998) developed 9 regression equations to relate soil water content values to prescribed matric head values by using the following general equation:

$$\theta(\psi) = 0.01\ (a\ OC + b\ silt + c\ clay + d) \quad (A22)$$

where a, b, c, d are the regression coefficients reported in Table A1.

Rawls et al. (1982) developed 12 regression equations to relate soil water content values to prescribed matric head values by using the following general equation:

$$\theta(\psi) = a + b\ sand + c\ silt + d\ clay + e\ OC + f\ \rho_b \quad (A23)$$

where a, b, c, d, e, f are the regression coefficients reported in Table A2.

Weynants et al. (2009) derived the parameters featuring in the van Genuchten equation (Eq. (1)):

$$\theta_s = 0.6355 + 0.0013\ clay - 0.1631\ \rho_b \quad (A24)$$

$$\theta_r = 0 \quad (A25)$$

$$\alpha = exp(-4.3003 - 0.0097\ clay + 0.0138\ sand - 0.0992\ OC) \quad (A26)$$

$$n = exp(-1.0846 - 0.0236\ clay - 0.0085\ sand + 1.3699\ 10^{-4}\ sand^2) + 1 \quad (A27)$$

where $OC = OM/1.724$ and $m = 1–1/n$.

ROSETTA was developed by Schaap et al. (2001) and is based on artificial neural network analysis (Zhang et al., 2020). ROSETTA is implemented in HYDRUS-1D (Šimůnek, 2013) and van Genuchten's parameters (α, n, θ_r, $\theta_{s,\ Ks}$) can be manually derived for each soil sample based on knowledge of sand, silt, clay and soil bulk density.

The euptfv2 prediction algorithms were derived with random forest method (Szabó et al., 2021) and are available through its web interface (https://doi.org/10.34977/euptfv2.01, Szabó et al., 2019a) and in the euptf2 R package from GitHub (https://doi.org/10.5281/zenodo.4281045, Weber et al., 2020). When soil depth, sand, silt, clay content, bulk density and organic carbon content were available, parameters of the van Genuchten model were computed with PTF07. When organic carbon was not available PTF03 could be used.

Prediction of saturated hydraulic conductivity

Wösten et al. (1999) derived saturated hydraulic conductivity, K_s (cm/d):

$$K_s = exp(7.755 + 0.0352silt + 0.93topsoil - 0.967\rho_b^2 - 0.000484clay^2 - 0.000322silt^2 + 0.001/silt - 0.0748/OM - 0.643ln(silt) - 0.01398\rho_b\ clay - 0.1673\rho_b\ OM + 0.02986topsoil\ clay - 0.03305topsoil\ silt) \quad (A28)$$

Weynants et al. (2009) derived the saturated hydraulic conductivity, K_0 (cm/d) fitted to measured hydraulic conductivity data:

$$K_0 = exp(1.9582 + 0.0308\ sand - 0.6142\ \rho_b - 0.1566OC) \quad (A29)$$

Since K_0 is different from K_s, we decided to predict K_s by using Eq. (5) with the vG parameters of WEY09 WRF.
Gupta et al. (2021) derived saturated hydraulic conductivity, K_s (cm/d) as follows:

$$K_s = 10\hat{(}1.44 + 2.053\rho_b - 1.256\rho_b^2 - 0.0533clay - 0.000051\rho_b clay + 0.00055clay^2 + 0.0079sand - 0.0008\rho_b sand + 0.000043clay\ sand + 0.000052sand^2) \quad (A30)$$

Cosby et al. (1984) obtained saturated hydraulic conductivity, K_s (cm/d):

$$K_s = 60.96\ 10\hat{(}0.0126\ sand - 0.0064clay - 0.60) \quad (A31)$$

Saxton and Rawls (2006) derived saturated hydraulic conductivity, K_s (cm/d):

$$\theta_{33t} = -0.251sand - 0.195clay + 0.011OM + 0.006(sand\ OM) - 0.027(clay\ OM) + 0.452(sand\ clay) + 0.299 \quad (A32)$$

$$\theta_{33} = \theta_{33t} + \left(1.283\theta_{33t}^2 - 0.374\theta_{33t} - 0.015\right) \quad (A33)$$

$$\theta_{1500t} = -0.024sand + 0.487clay + 0.006OM + 0.005(sand\ OM) - 0.013(clay\ OM) + 0.068(sand\ clay) + 0.031 \quad (A34)$$

$$\theta_{1500} = \theta_{1500t} + (0.14\theta_{1500t} - 0.02) \quad (A35)$$

$$\theta_{(S-33)t} = 0.278sand + 0.034clay + 0.022OM - 0.018(sand\ OM) - 0.027(clay\ OM) - 0.584(sand\ clay) + 0.078 \quad (A36)$$

$$\theta_{S-33} = \theta_{(S-33)t} + (0.636\theta_{(S-33)t} - 0.107) \quad (A37)$$

$$\theta_s = \theta_{33} + \theta_{S-33} - 0.097sand + 0.043 \quad (A38)$$

$$\lambda = (ln(\theta_{33}) - ln(\theta_{1500}))/(ln(1500) - ln(33)) \quad (A39)$$

$$K_s = 4632(\theta_s - \theta_{33})^{(3-\lambda)} \quad (A40)$$

Araya and Ghezzehei (2019) derived pedotransfer functions with machine learning methods for the prediction of saturated hydraulic conductivity, K_s (cm/d). From those PTFs the best performing boosted-regression-tree-based algorithm was applied to compute K_s from sand, silt and clay content, bulk density and soil organic carbon content, called fGBM_32. When organic carbon content was not available fGBM_31 was applied.

For the estimation of K_s with euptfv2, PTF02 was applied, which uses soil depth, sand, silt, clay and organic carbon content as predictors. When organic carbon content was missing PTF01 could be used.

Appendix B. Supplementary data

Supplementary material related to this article can be found, in the online version, at doi:https://doi.org/10.1016/j.ejrh.2021.100903.

References

Abkenar, F.Z., Rasoulzadeh, A., 2019. Functional evaluation of pedotransfer functions for simulation of soil profile drainage. Irrig. Drain. 68, 573–587.

Araya, S.N., Ghezzehei, T.A., 2019. Using machine learning for prediction of saturated hydraulic conductivity and its sensitivity to soil structural perturbations. Water Resour. Res. 55, 5715–5737.

Arya, L.M., Paris, J.F., 1981. A physicoempirical model to predict the soil moisture characteristic from particle-size distribution and bulk density data. Soil Sci. Soc. Am. J. 45, 1023–1030.

Assouline, S., Or, D., 2014. The concept of field capacity revisited: defining intrinsic static and dynamic criteria for soil internal drainage dynamics. Water Resour. Res. 50. https://doi.org/10.1002/2014WR015475.

Batjes, N.H., Ribeiro, E., van Oostrum, A., 2020. Standardised soil profile data to support global mapping and modelling (WoSIS snapshot 2019). Earth Syst. Sci. Data 299–320. https://doi.org/10.5194/essd-12-299-2020.

Beven, K., 2013. So how much of your error is epistemic? Lessons from Japan and Italy. Hydrol. Process. 27, 1677–1680.

Brooks, R.H., Corey, A.J., 1964. Hydraulic properties of porous media. Hydrol. Paper 3. Colorado State Univ., Fort Collins.

Bruand, A., Baize, D., Hardy, M., 1994. Prediction of water retention properties of clayey soils: validity of relationships using a single soil characteristic. Soil Use Manage. 10, 99–103.

Campbell, G.S., Shiozawa, S., 1992. Prediction of hydraulic properties of soils using particle-size distribution and bulk density data. Indirect Methods for Estimating the Hydraulic Properties of Unsaturated Soils. University of California, Riverside, pp. 317–328.

Canarache, A., 1993. Physical-technological maps—a possible product of soil survey for direct use in agriculture. Soil Technol. 6, 3–16.

Christiansen, K., Feyen, J., 2001. Analysis of uncertainties associated with different methods to determine soil hydraulic properties and their propagation in the distributed hydrological MIKE SHE model. J. Hydrol. 246, 63–81.

Ciollaro, G., Romano, N., 1995. Spatial variability of the hydraulic properties of a volcanic soil. Geoderma 65, 263–282.

Cornelis, W.M., Ronsyn, J., Van Meirvenne, M., Hartmann, R., 2001. Evaluation of pedotransfer functions for predicting the soil moisture retention curve. Soil Sci. Soc. Am. J. 65, 638–648.

Cosby, B.J., Hornberger, G.M., Clapp, R.B., Ginn, T.R., 1984. A statistical exploration of the relationships of soil moisture characteristics to the physical properties of soils. Water Resour. Res. 20, 682–690.

Dane, J.H., Hopmans, J.W., 2002. Water retention and storage. In: Dane, J.H., Topp, G.C. (Eds.), Methods of Soil Analysis, Part 4, SSSA Book Ser. 5. SSSA, Madison, Wis, pp. 671–675.

de Sousa, L.M., Poggio, L., Batjes, N.H., Heuvelink, G.B.M., Kempen, B., Ribeiro, E., Rossiter, D., 2021. SoilGrids 2.0: producing soil information for the globe with quantified spatial uncertainty. Soil 7, 217–240.

De Vos, B., Van Meirvenne, M., Quataert, P., Deckers, J., Muys, B., 2005. Predictive quality of pedotransfer functions for estimating bulk density of forest soils. Soil Sci. Soc. Am. J. 69, 500–510.

Diks, C.G.H., Vrugt, J.A., 2010. Comparison of point forecast accuracy of model averaging methods in hydrologic applications, Stochastic Environ. Res. Risk Assess. 24, 809–821.

Eck, D.V., Qin, M., Hirmas, D.R., Giménez, D., Brunsell, N.A., 2016. Relating quantitative soil structure metrics to saturated hydraulic conductivity. Vadose Zone J. 15. https://doi.org/10.2136/vzj2015.05.0083.

Figueras, J., Gribb, M.M., 2009. Design of a user-friendly automated multistep outflow apparatus. Vadose Zone J. 8, 523–529.

Gee, G.W., Or, D., 2002. Particle-size analysis. In: Dane, J.H., Topp, G.C. (Eds.), Methods of Soil Analysis. Part 4. SSSA Book Series No. 5. SSSA, Madison, WI, pp. 255–293.

Ghanbarian, B., Hunt, A.G., Skaggs, T.H., Jarvis, N., 2017. Upscaling soil saturated hydraulic conductivity from pore throat characteristics. Adv. Water Resour. 104, 105–113.

Guarracino, L., 2007. Estimation of saturated hydraulic conductivity Ks from the van Genuchten shape parameter α. Water Resour. Res. 43, W11502 https://doi.org/10.1029/2006WR005766.

Guber, A.K., Pachepsky, Ya.A., van Genuchten, M.Th., Rawls, W.J., Šimůnek, J., Jacques, D., Nicholson, T.J., Cady, R.E., 2006. Field-scale water flow simulations using ensembles of pedotransfer functions for soil water retention. Vadose Zone J. 5, 234–247. https://doi.org/10.2136/vzj2005.0111.

Guber, A.K., Pachepsky, Ya.A., van Genuchten, M.Th., Šimůnek, J., Jacques, D., Nemes, A., Nicholson, T.J., Cady, R.E., 2009. Multimodel simulation of water flow in a field soil using Pedotransfer Functions. Vadose Zone J. 8, 1–10.

Gupta, S., Larson, W.E., 1979. Estimating soil water retention characteristics from particle size distribution, organic matter percent, and bulk density. Water Resour. Res. 15, 1633–1635.

Gupta, S., Hengl, T., Lehmann, P., Bonetti, S., Or, D., 2021. SoilKsatDB: global database of soil saturated hydraulic conductivity measurements for geoscience applications. Earth Syst. Sci. Data 13, 1593–1612.

Haghverdi, A., Cornelis, W.M., Ghahraman, B., 2012. A pseudo-continuous neural network approach for developing water retention pedotransfer functions with limited data. J. Hydrol. 442–443, 46–54.

Haverkamp, R.T., Parlange, J.Y., 1986. Predicting the water-retention curve from particle-size distribution: sandy soils without organic matter. Soil Sci. 142, 325–339.

Haverkamp, R., Zammit, C., Boubkraoui, F., Rajkai, K., Arrúe, J.L., Heckmann, N., 1997. GRIZZLY, Grenoble Soil Catalogue: Soil Survey of Field Data and Description of Particle-size, Soil Water Retention and Hydraulic Conductivity Functions. Laboratoire d'Etude des Transferts en Hydrologie et en Environment, Grenoble, France.

Hengl, T., Mendes de Jesus, J., Heuvelink, G.B.M., Ruiperez Gonzalez, M., Kilibarda, M., Blagotìc, A., Shangguan, W., Wright, M.N., Geng, X., Bauer-Marschallinger, B., Guevara, M.A., Vargas, R., MacMillan, R.A., Batjes, N.H., Leenaars, J.G.B., Ribeiro, E., Wheeler, I., Mantel, S., Kempen, B., 2017. SoilGrids250m: global gridded soil information based on machine learning. PLoS One 12, e0169. https://doi.org/10.1371/journal.pone.0169748, 748.

Hopmans, J.W., Šimůnek, J., Romano, N., Durner, W., 2002. Inverse methods. In: Dane, J.H., Topp, G.C. (Eds.), Methods of Soil Analysis. Part 4. SSSA Book Series No. 5. SSSA, Madison, WI, pp. 963–1008.

Ilek, A., Kucza, J., Witek, W., 2019. Using undisturbed soil samples to study how rock fragments and soil macropores affect the hydraulic conductivity of forest stony soils: some methodological aspects. J. Hydrol. 570, 132–140.

Kotlar, A.M., Jong van Lier, Q., Barros, A.H.C., Iversen, B.V., Vereecken, H., 2019. Development and uncertainty assessment of pedotransfer functions for predicting water contents at specific pressure heads. Vadose Zone J. 18, 190063.

Laliberte, G.E., Brooks, R.H., Corey, A.T., 1968. Permeability calculated from desaturation data. J. Irrig. Drain. Div. Proc. ASCE 94, 57–71.

Li, X., Li, J.H., Zhang, L.M., 2014. Predicting bimodal soil–water characteristic curves and permeability functions using physically based parameters. Comput. Geotech. 57, 85–96.

Liao, K.-H., Xu, S.-H., Wu, J.-C., Ji, S.-H., Lin, Q., 2011. Assessing soil water retention characteristics and their spatial variability using pedotransfer functions. Pedosphere 21, 413–422.

Lilly, A., Nemes, A., Rawls, W.J., Pachepsky, Y.A., 2008. Probabilistic approach to the identification of input variables to estimate hydraulic conductivity. Soil Sci. Soc. Am. J. 72, 16–24.

Mebius, L.J., 1960. A rapid method for the determination of organic carbon in soil. Anal. Chim. Acta 22, 120–124.

Minasny, B., Hartemink, A.E., 2011. Predicting soil properties in the tropics. Earth Sci. Rev. 106, 52–62.

Minasny, B., McBratney, A.B., 2003. Integral energy as a measure of soil-water availability. Plant Soil 249, 253–262.

Mohammadi, M.H., Meskini-Vishkaee, F., 2013. Predicting soil moisture characteristic curves from continuous particle-size distribution data. Pedosphere 23 (1), 70–80.

Mohammadi, M.H., Vanclooster, M., 2011. Predicting the soil moisture characteristic curve from particle size distribution with a simple conceptual model. Vadose Zone J. 10, 594–602.

Mualem, Y., 1976. A new model for predicting the hydraulic conductivity of unsaturated porous media. Water Resour. Res. 12, 513–522.
Nasta, P., Romano, N., 2016. Use of a flux-based field capacity criterion to identify effective hydraulic parameters of layered soil profiles subjected to synthetic drainage experiments. Water Resour. Res. 52, 566–584.
Nasta, P., Huynh, S., Hopmans, J.W., 2011. Simplified multistep outflow method to estimate unsaturated hydraulic functions for coarse-textured soils. Soil Sci. Soc. Am. J. 75, 418–425.
Nasta, P., Vrugt, J.A., Romano, N., 2013. Prediction of the saturated hydraulic conductivity from Brooks and Corey's water retention parameters. Water Resour. Res. 49. https://doi.org/10.1002/wrcr.20269.
Nasta, P., Boaga, J., Deiana, R., Cassiani, G., Romano, N., 2019. Comparing ERT- and scaling-based approaches to parameterize soil hydraulic properties for spatially distributed model applications. Adv. Water Resour. 126, 155–167.
Nemes, A., Schaap, M.G., Wösten, J.H.M., 2003. Functional evaluation of pedotransfer functions derived from different scales of data collection. Soil Sci. Soc. Am. J. 67, 1093–1102.
Nimmo, J.R., Herkelrath, W.N., Laguna Luna, A.M., 2007. Physically based estimation of soil water retention from textural data: general framework, new models, and streamlined existing models. Vadose Zone J. 6, 766–773.
Oosterveld, M., Chang, C., 1980. Empirical relations between laboratory determinations of soil texture and moisture characteristic. Can. Agric. Eng. 22, 149–151.
Peters, A., Durner, W., 2008. Simplified evaporation method for determining soil hydraulic properties. J. Hydrol. 356, 147–162.
Peters, A., Durner, W., Wessolek, G., 2011. Consistent parameter constraints for soil hydraulic functions. Adv. Water Resour. 34, 1352–1365.
Petersen, G.W., Cunningham, R.L., Matelski, R.P., 1968. Moisture characteristics of Pennsylvania soils: I. Moisture retention as related to texture. Soil Sci. Soc. Am. Proc. 32, 271–275.
Pringle, M.J., Romano, N., Minasny, B., Chirico, G.B., Lark, R.M., 2007. Spatial evaluation of pedotransfer functions using wavelet analysis. J. Hydrol. 333, 182–198.
R Core Team, 2020. R: A Language and Environment for Statistical Computing. R Foundation for Statistical Computing, Vienna, Austria. https://www.R-project.org/.
Rawls, W.J., Brakensiek, D.L., 1985. Prediction of soil water properties for hydrologic modeling. In: Jones, E.B., Ward, T.J. (Eds.), Proc. Symp. Watershed Management in the Eighties. Denver, CO. 30 Apr.–1 May 1985. Am. Soc. Civil Eng., New York, pp. 293–299.
Rawls, W.J., Brakensiek, D.L., Saxton, K.E., 1982. Estimation of soil water properties. Trans. ASAE 25, 1316–1320.
Reynolds, W.D., Elrick, D.E., 2002. Pressure infiltrometer. In: Dane, J.H., Topp, G.C. (Eds.), Methods of Soil Analysis: Part 4. Physical Methods. Soil Sci. Soc. Am., Inc., Madison, WI, pp. 826–836.
Romano, N., 1993. Use of an inverse method and geostatistics to estimate soil hydraulic conductivity for spatial variability analysis. Geoderma 60, 169–186.
Romano, N., 2004. Spatial structure of PTF estimates. In: Pachepsky, Y.A., Rawls, W.J. (Eds.), Development of Pedotransfer Functions in Soil Hydrology. Elsevier Science, Amsterdam, pp. 273–294.
Romano, N., Nasta, P., 2016. How effective is bimodal soil hydraulic characterization? Functional evaluations for predictions of soil water balance. Eur. J. Soil Sci. 67, 523–535.
Romano, N., Palladino, M., 2002. Prediction of soil water retention using soil physical data and terrain attributes. J. Hydrol. 265, 56–75.
Romano, N., Santini, A., 1997. Eff ;ectiveness of using pedo-transfer functions to quantify the spatial variability of soil water retention characteristics. J. Hydrol. 202, 137–157.
Romano, N., Santini, A., 2002. Water retention and storage: Field. In: Dane, J.H., Topp, G.C. (Eds.), Methods of Soil Analysis, Part 4, Physical Methods. SSSA Book Series N.5, Madison, WI, USA, pp. 721–738. ISBN 0-89118-841-X.
Romano, N., Hopmans, J.W., Dane, J.H., 2002. Water retention and storage: suction table. In: Dane, J.H., Topp, G.C. (Eds.), Methods of Soil Analysis, Part 4, Physical Methods. SSSA Book Series N.5, Madison, WI, USA, pp. 692–698. https://doi.org/10.2136/sssabookser5.4.c25. ISBN 0-89118-841-X.
Romano, N., Palladino, M., Chirico, G.B., 2011. Parameterization of a bucket model for soil-vegetation-atmosphere modeling under seasonal climatic regimes. Hydrol. Earth Syst. Sci. 15, 3877–3893.
Romano, N., Nasta, P., Bogena, H.R., De Vita, P., Stellato, L., Vereecken, H., 2018. Monitoring hydrological processes for land and water resources management in a Mediterranean ecosystem: the Alento River catchment observatory. Vadose Zone J. 17, 180042 https://doi.org/10.2136/vzj2018.03.0042.
Rudiyanto, Minasny, B., Chaney, N.W., Maggi, F., Giap, S.G.E., Shah, R.M., Fiantis, D., Setiawan, B.I., 2021. Pedotransfer functions for estimating soil hydraulic properties from saturation to dryness. Geoderma 403, 115194. https://doi.org/10.1016/j.geoderma.2021.115194.
Saxton, K.E., Rawls, W.J., 2006. Soil water characteristic estimates by texture and organic matter for hydrologic solutions. Soil Sci. Soc. Am. J. 70, 1569–1578.
Saxton, K.E., Rawls, W.J., Romberger, J.S., Papendick, R.I., 1986. Estimating generalized soil-water characteristics from texture. Soil Sci. Soc. Am. J. 50, 1031–1036.
Schaap, M.G., Leij, F.J., 2000. Improved prediction of unsaturated hydraulic conductivity with the Mualem–van Genuchten model. Soil Sci. Soc. Am. J. 64, 843–851.
Schaap, M.G., Leij, F.J., van Genuchten, M.T., 2001. ROSETTA: a computer program for estimating soil hydraulic parameters with hierarchical pedotransfer functions. J. Hydrol. 251, 163–176.
Schelle, H., Iden, S.C., Peters, A., Durner, W., 2010. Analysis of the agreement of soil hydraulic properties obtained from Multistep-Outflow and Evaporation methods. Vadose Zone J. 9, 1080–1091.
Schindler, U., Müller, L., 2006. Simplifying the evaporation method for quantifying soil hydraulic properties. J. Plant Nutr. Soil Sci. 169, 623–629.
Silva, A.C., Armindo, R.A., Brito, A.S., Schaap, M.G., 2017. An assessment of pedotransfer function performance for the estimation of spatial variability of key soil hydraulic properties. Vadose Zone J. 16, 1–10.
Šimůnek, J., Šejna, M., van Genuchten, M.T., 2018. Recent developments and applications of the HYDRUS computer software packages. Vadose Zone J. https://doi.org/10.2136/vzj2016.04.0033.
Sing, A., Haghverdi, A., Öztürk, H.S., Durner, W., 2020. Developing pseudo continuous Pedotransfer Functions for international soils measured with the evaporation method and the HYPROP system: I. The soil water retention curve. Water 12, 3425. https://doi.org/10.3390/w12123425.
Szabó, B., Gyurkó, D., Weynants, M., Weber, T.K., 2019a. Web Interface for European Hydraulic Pedotransfer Functions (euptfv2). At: https://ptfinterface.rissac.hu/. (Accessed 17 September 2020).
Szabó, B., Szatmári, G., Takács, K., Laborczi, A., Makó, A., Rajkai, K., Pásztor, L., 2019b. Mapping soil hydraulic properties using random-forest-based pedotransfer functions and geostatistics. Hydrol. Earth Syst. Sci. 23, 2615–2635. https://doi.org/10.5194/hess-23-2615-2019.
Szabó, B., Weynants, M., Weber, T.K., 2021. Updated european hydraulic pedotransfer functions with communicated uncertainties in the predicted variables (euptfv2). Geosci. Model Dev. 14, 151–175. https://doi.org/10.5194/gmd-14-151-2021.
Tietje, O., Tapkenhinrichs, M., 1993. Evaluation of pedo-transfer functions. Soil Sci. Soc. Am. J. 57, 1088–1095.
Tomasella, J., Hodnett, M.G., 1998. Estimating soil water retention characteristics from limited data in Brazilian Amazonia. Soil Sci. 163, 190–202.
Topp, G.C., Ferré, P.A., 2002. Water content. In: Dane, J.H., Topp, G.C. (Eds.), Methods of Soil Analysis. Part 4. SSSA Book Ser. 5. SSSA, Madison, WI, pp. 417–545.
Torres, L.C., Keller, T., de Lima, R.P., Tormena, C.A., de Lima, H.V., Giarola, N.F.B., 2021. Impacts of soil type and crop species on permanent wilting of plants. Geoderma 384, 114798. https://doi.org/10.1016/j.geoderma.2020.114798.
Twarakavi, N.K.C., Sakai, M., Šimůnek, J., 2009. An objective analysis of the dynamic nature of field capacity. Water Resour. Res. 45, W10410 https://doi.org/10.1029/2009WR007944.
van Genuchten, M.Th., 1980. A closed form equation for predicting the hydraulic conductivity of unsaturated soils. Soil Sci. Soc. Am. J. 44, 892–898.
Van Looy, K., Bouma, J., Herbst, M., Koestel, J., Minasny, B., Mishra, U., et al., 2017. Pedotransfer functions in Earth system science: Challenges and perspectives. Rev. Geophys. 55, 1199–1256. https://doi.org/10.1002/2017RG000581.
Vereecken, H., Maes, J., Feyen, J., Darius, P., 1989. Estimating the soil moisture retention characteristics from texture, bulk density and carbon content. Soil Sci. 148, 389–403.
Vereecken, H., Diels, J., Van Orshoven, J., Feyen, J., Bouma, J., 1992. Functional evaluation of pedotransfer functions for the estimation of soil hydraulic properties. Soil Sci. Soc. Am. J. 56, 1371–1378.
Wackernagel, H., 2003. Multivariate Geostatistics, 3rd edition. Springer-Verlag, Berlin.
Weber, T.K.D., Weynants, M., Szabó, B., 2020. R Package of Updated European Hydraulic Pedotransfer Functions (euptf2). https://doi.org/10.5281/zenodo.4281045.

Weihermüller, L., Herbst, M., Javaux, M., Weynants, M., 2017. Erratum to revisiting Vereecken pedotransfer functions: introducing a closed-form hydraulic model. Vadose Zone J. 16 (1) https://doi.org/10.2136/vzj2008.0062er.

Weynants, M., Vereecken, H., Javaux, M., 2009. Revisiting Vereecken pedotransfer functions: introducing a closed-form hydraulic model. Vadose Zone J. 8 (1), 86–95. https://doi.org/10.2136/vzj2008.0062.

Weynants, M., Montanarella, L., Tóth, G., Arnoldussen, A., Anaya Romero, M., Bilas, G., Borresen, T., Cornelis, W., Daroussin, J., Gonçalves, M.D.C., Haugen, L.-E., Hennings, V., Houskova, B., Iovino, M., Javaux, M., Keay, C.A., Kätterer, T., Kvaerno, S., Laktinova, T., Lamorski, K., Lilly, A., Mako, A., Matula, S., Morari, F., Nemes, A., Patyka, N.V., Romano, N., Schindler, U., Shein, E., Slawinski, C., Strauss, P., Tóth, B., Woesten, H., 2013. European HYdropedological Data Inventory (EU-HYDI), EUR – Scientific and Technical Research Series. ISSN 1831-9424, Luxembourg.

Wösten, J.H.M., Lilly, A., Nemes, A., Le Bas, C., 1999. Development and use of a database of hydraulic properties of European soils. Geoderma 90, 169–185.

Zhang, Y., Schaap, M.G., 2017. Weighted recalibration of the Rosetta pedotransfer model with improved estimates of hydraulic parameter distributions and summary statistics (Rosetta3). J. Hydrol. 547, 39–53. https://doi.org/10.1016/j.jhydrol.2017.01.004.

Zhang, Y., Schaap, M.G., 2019. Estimation of saturated hydraulic conductivity with pedotransfer functions: a review. J. Hydrol. 575, 1011–1030. https://doi.org/10.1016/j.jhydrol.2019.05.058.

Zhang, X., Wendroth, O., Matocha, C., Zhu, J., Reyes, J., 2020. Assessing field-scale variability of soil hydraulic conductivity at and near saturation. Catena 187, 104335. https://doi.org/10.1016/j.catena.2019.104335.